Chapter 3
Thermal Conductivity of Particulate Nanocomposites

Jose Ordonez-Miranda, Ronggui Yang, and Juan Jose Alvarado-Gil

Abstract The modeling of the thermal conductivity of composites made up of metallic and non-metallic micro/nanoparticles embedded in a solid matrix is discussed in detail, at both the dilute and non-dilute limits of particle concentrations. By modifying both the thermal conductivity of the matrix and particles, to take into account the strong scattering of the energy carriers with the surface of the nanoparticles, it is shown that the particle size effect shows up on the thermal conductivity of nanocomposites through: (1) the collision cross-section per unit volume of the particles and, (2) the mean distance that the energy carriers can travel inside the particles. The effect of the electron–phonon interactions within metallic particles shows up through the reduction of the thermal conductivity of these particles with respect to its values obtained under the Fourier law approach. The thermal conductivity of composites with metallic particles depend strongly on (1) the relative size of the particles with respect to the intrinsic coupling length, and (2) the ratio between the electron and phonon thermal conductivities. The obtained results have shown that the size dependence of the composite thermal conductivity appears not only through the interfacial thermal resistance but also by means of the electron–phonon coupling. Furthermore, at the non-dilute limit, the interaction among the particles is taken into account through a crowding factor,

J. Ordonez-Miranda
Laboratoire d'Énergétique Moléculaire et Macroscopique, Combustion, UPR CNRS 288, Ecole Centrale Paris, Grande Voie des Vignes, 92295 Châtenay Malabry, France
e-mail: jose.ordonez@ecp.fr

R. Yang (✉)
Department of Mechanical Engineering, University of Colorado, Boulder, CO 80309, USA
e-mail: Ronggui.Yang@Colorado.Edu

J.J. Alvarado-Gil
Department of Applied Physics, Centro de Investigación y de Estudios Avanzados del I.P.N-Unidad Mérida, Carretera Antigua a Progreso km. 6, A.P. 73 Cordemex, Mérida, Yucatán 97310, Mexico
e-mail: jjag@mda.cinvestav.mx

X. Wang and Z.M. Wang (eds.), *Nanoscale Thermoelectrics*, Lecture Notes in Nanoscale Science and Technology 16, DOI 10.1007/978-3-319-02012-9_3,

which is determined by the effective volume of the particles. The proposed crowding factor model is able to capture accurately the effect of the interactions among the particles for concentrations up to the maximum packing fraction of the particles. The predictions of the obtained analytical models are in good agreement with available experimental and numerical data and they can be applied to guide the design and improve the thermal performance of composite materials.

3.1 Introduction

Composites based on the dispersion of a discontinuous phase of particles embedded in a continuous matrix, have been used for more than a hundred years, due to their outstanding properties that often cannot be obtained with single-phase materials [1, 2]. In many applications ranging from mechanical structures to electronics, it is common to engineer material properties by combining the most useful properties of two or more phases. The prediction and understanding of the composite properties has been a complex subject of research since the properties of composite materials depend on a number of structural parameters and physical/chemical properties including the volume fraction, size, shape and orientation of the particles as well as the interfacial characteristics between the particles and matrix. The two basic configurations of the particles in composites are defined by the random and aligned distribution of particle inclusions, as shown in Fig. 3.1a, b, respectively. The overall thermal conductivity of the first composite can be considered as isotropic, while the thermal conductivity of the second one could be anisotropic.

Since Maxwell [3] who presented a theoretical basis for calculating the effective thermal conductivity of particulate composites, a considerable amount of theoretical and empirical approaches have been employed to analyze the thermal conductivity of composites, as summarized in the books by Milton [1] and Torquato [2], and references therein [4–15], in which most analysis has been performed based on an effective medium approximation (EMA), under the framework of the Fourier law of heat conduction. One of the most widely-used models was recently derived by Nan et al. [8], who considered spheroidal inclusions with interfacial thermal resistance and generalized the previous results of Benveniste [4], and Hasselman and Johnson [5], for spherical, cylindrical and flat-plate inclusions. These EMA models can predict reasonably well the thermal conductivity of composites with small volume fraction of macro/micro-sized particles where heat conduction is governed by the Fourier law.

However, the EMA models developed earlier have not considered the details of heat-carrying carriers and their interaction with microstructures. As a consequence, there are three major drawbacks of these classical models based on the Fourier's law: (1) They are not appropriate for predicting the thermal conductivity of nanocomposites where the particle size could be of the order or smaller than the mean free path of the energy carriers [13, 16, 17]. (2) They do not consider the effect of the electron–phonon coupling and therefore they are not applicable for

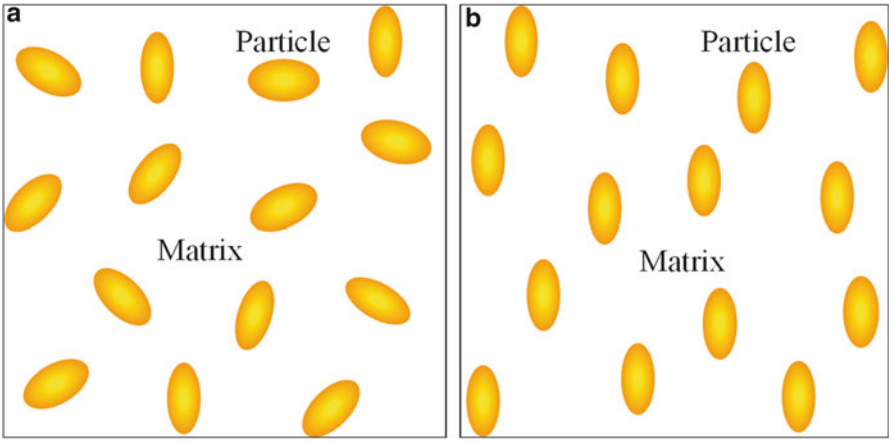

Fig. 3.1 Schematics of a composite with (**a**) random and (**b**) aligned distribution of particles

composites with metallic particles, where the heat conduction is due to the flow of the electron and phonon gases and their interactions. (3) They do not consider the effect of the interaction among the particles and therefore they are not applicable for high concentration of particles (typically larger than 15 %).

In this chapter, we present in detail the modeling of the thermal conductivity of composites made up of metallic and non-metallic micro/nanoparticles embedded in a solid matrix, at both the dilute and non-dilute limits of particle concentrations, which essentially addresses the above drawbacks. Before we present the detailed modeling, we summarize in the rest of this section the basic physics behind the drawbacks identified above. Section 3.2 is dedicated to address the size effects of energy carriers in nanocomposites. A thermal conductivity model for metal-nonmetal composites is developed in Sect. 3.3, which takes into account the effects of both electron–phonon coupling and thermal boundary resistance. In Sect. 3.4, a crowding factor model is presented that can be utilized to extend the thermal conductivity models at the dilute limit to high concentrations. Section 3.5 concludes this chapter.

3.1.1 On the Nanocomposites

Significant interest has recently been given to composites with nano-sized particles (nanocomposites), due to their importance in electronics, structural and energy applications [16]. In contrast to the composites with micro-sized particles, the heat conduction through nanocomposites is expected to be strongly determined by the interface/surface effects. The energy carriers (electrons and phonons) in composites experience multiple scattering processes, which ultimately determine the effective thermal conductivity of the material. One of these scattering

mechanisms is defined by the collision of the energy carriers with the surface of the embedded particles and its effects are strongly determined by the relative size of the particles with respect to the intrinsic mean free path (MFP) associated with the scattering among carriers and carriers with natural impurities. When the size of the particles is much larger than the intrinsic MFP, the collisions of the energy carriers with the surface of the particles is quite infrequent in comparison with the other scattering processes, and therefore their effects can be neglected. By contrast, if the size of the particles is of the order of the MFP or smaller, these collisions can be very frequent and hence their contribution to the heat conduction is significant. Considering that the MFP of electrons and phonons are in the order of a few nanometers to hundreds of nanometers, in a wide variety of materials at room temperature, the effects of the size of the particles are expected to be negligible for micro-sized or bigger particles and become significant for nano-sized particles.

3.1.2 On the Composites with Metallic Particles

Metals usually have much higher thermal conductivities than ceramic or polymer materials. It is expected that metallic nanoparticles can significantly enhance the thermal conductivity of the matrix material [1]. Despite of its importance and practice in using metallic fillers for composite materials, currently there exist no models that can correctly describe the heat transport through nanocomposites with metallic particles in dielectric materials. Heat transport through metallic particles, in contrast to that in nonmetallic materials, is not only due to the phonon gas but also due to the electron gas and their interactions [18]. In addition to the electron–electron and phonon-phonon scatterings, the electron–phonon interactions are also present in metals. In fact, the coupling between electrons and phonons inside the metallic particles and their interaction with the matrix has a dominant role in the heat transport through the composites. In addition, as the size of the particles reduces to nanoscale, the frequent collisions of the electrons and phonons with the surface of the embedded particles significantly shortens their effective mean free path, as shown in Fig. 3.2, which further complicates the modeling of the effective thermal conductivity of metal-nonmetal composite.

3.1.3 On the High Particle Concentrations

Most existing models for thermal conductivity of composites have assumed that the volume fraction of the particles is small enough (typically smaller than 15 %) that the interactions among the particles can be neglected. In such dilute limit, the heat flux lines generated by one particle are not distorted by the presence of the neighboring particles when the distance between neighboring particles is much larger than their size, as shown in Fig. 3.3a. However, for higher particle

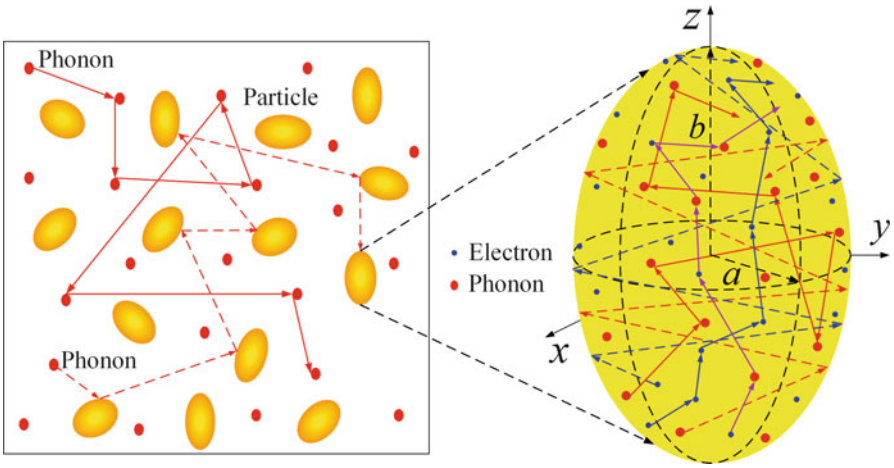

Fig. 3.2 Schematics of the different scattering processes of the energy carriers inside the nonmetal matrix and the metallic particles of a composite

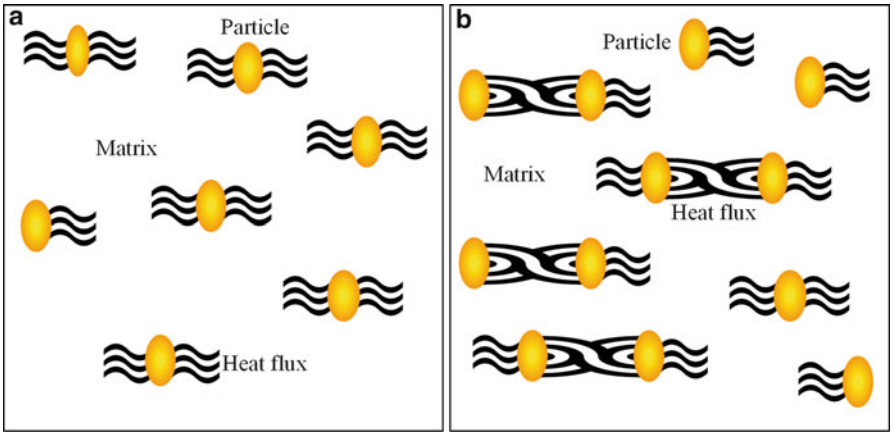

Fig. 3.3 Schematics of the lines of the heat flux inside a composite with a (**a**) dilute and (**b**) non-dilute concentration of particles

concentrations, the distance between neighboring particles can be of the order of the particle size or smaller and the interaction among particles have to be considered, which results in distortion in heat flux that is different from the prediction of single particle assumption, as shown in Fig. 3.3b. Due to this particle interaction, the modeling of the thermal conductivity of composites at the non-dilute limit has been a challenging research problem.

3.2 Size Effects in Nanocomposites

Theoretical models predicting the thermal conductivity of nanocomposites and explaining how the nanoscale structures influence the bulk thermal properties are scarce. Models for thermal conductivity of semiconductor and dielectric nanocomposites just start to emerge. By calculating the scattering cross section and the relaxation time due to a single particle, Khitun et al. [9] derived an expression for the thermal conductivity of a composite with periodically arranged nanoparticles. Even though they reported a particle-size dependence of the effective thermal conductivity, their approach is limited to elastic scattering inside the particles and specular scattering at the interfaces. More recently, based on the phonon Boltzmann transport equation (BTE), Yang et al. [14–16, 19–21] studied the phonon thermal conductivity of a variety of nanocomposites. Their simulations showed that the temperature profiles in nanocomposites are very different from those in conventional composites due to the ballistic phonon transport at nanoscale. This indicates that the dependence of the thermal conductivity on the particle size and volume fraction in nanocomposites can be significantly different from that of macro/micro-composites. Along the same line, Prasher [11, 22] derived semi-analytical expressions for the effective thermal conductivity of nanocomposites with aligned nanowires. More recently, Minnich and Chen [13] proposed a modified EMA formulation based on Nan et al. model [8] by considering the interfacial scattering of phonons in nanocomposites. The predictions of this modified EMA for the thermal conductivity of composites reinforced with spherical and cylindrical particles, as a function of the interface density, are in good agreement with the numerical approaches based on the BTE and Monte Carlo (MC) simulations. We have recently extend the formalism proposed by Minnich and Chen [13] for nanocomposites with spheroidal inclusions. Our results exhibit an explicit dependence of the composite thermal conductivity on the collision cross-section per unit volume of the particles and the average distance that the energy carriers can travel inside the particles.

3.2.1 Modified Effective Medium Approximation (MEMA) Model

In general, the thermal conductivity k of composites can be written as,

$$k = k(k_m, k_I, f, P), \tag{3.1}$$

where k_m and k_I are the thermal conductivities of the matrix and the particles, respectively; f is the volume fraction of the particles and P stands for other properties as the particles size, shape and orientation, and the interfacial thermal resistance. The classical models [4, 5, 8, 12] derived under the framework of the

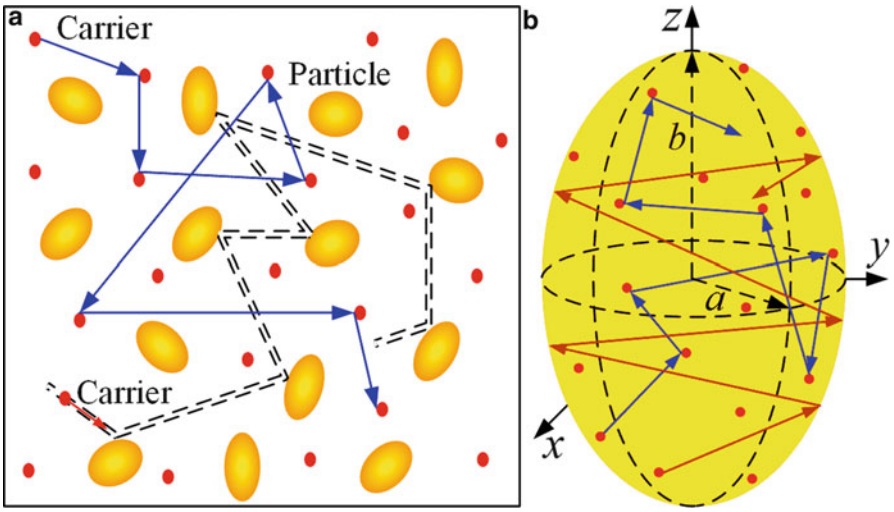

Fig. 3.4 Schematics showing the scattering process of an energy carrier inside (**a**) the matrix and (**b**) the spheroidal particle

Fourier law of heat conduction have the form of (3.1), and they consider k_m and k_I as the bulk thermal conductivity of the constituents. To take into account the particle size effects, the thermal conductivity of the matrix and the particles needs to be modified, by determining the effective mean free path of the energy carriers associated with all the scattering processes. These calculations have been proposed and developed by Minnich and Chen [13] for spherical and cylindrical nanoparticles, and subsequently they have been extended for spheroidal particles by Ordonez-Miranda et al. [23].

According to the kinetic theory [24], the thermal conductivity of a material is given by

$$k_\xi = \frac{1}{3}\int C_\xi(\varepsilon) v_\xi(\varepsilon) l_\xi(\varepsilon) d\varepsilon, \tag{3.2}$$

where C_ξ, v_ξ and l_ξ are the volumetric heat capacity per unit energy, the group velocity and the total MFP of electrons ($\xi = e$) or phonons ($\xi = p$). For a composite as shown in Fig. 3.4a, the MFP of the energy carriers in the matrix is not only determined by the intrinsic carrier-carrier scatterings but also by the carrier-boundary collisions. According to the Matthiessen rule [24], the effective MFP $l_{\xi,m}$ of the energy carriers in the matrix can be written by

$$\frac{1}{l_{\xi,m}} = \frac{1}{l_{\xi\xi,m}} + \frac{1}{l_{\xi I,m}} \tag{3.3}$$

where $l_{\xi I,m}$ is the MFP associated with the collisions of the energy carriers with the outer surface of the particles, and it is assumed to be independent of the intrinsic scattering of the energy carriers represented by $l_{\xi\xi,m}$.

To determine $l_{\xi I,m}$, let us define $A_\perp$ as the collision cross-section (the effective area of collision) between an energy carrier and a particle, and n as the number of particles per unit volume of them (the density of particles). If V is the volume of one particle, the volume fraction of particles is $f = nV$. Now if one energy carrier travels a distance L, it collides with particles within the cylindrical swept volume $A_\perp L$, which contains $nA_\perp L$ particles (see the dashed lines in Fig. 3.3a). The MFP $l_{\xi I,m}$ due to particle inclusions can be thus written as

$$l_{\xi I,m} = \frac{L}{nA_\perp L} = \frac{1}{nA_\perp} = \frac{1}{\sigma_\perp f}, \tag{3.4}$$

where $\sigma_\perp = A_\perp/V$ is the collision cross-section per unit volume of one particle. After replacing (3.3) and (3.4) into (3.2), it is found that the thermal conductivity $k_{\xi,m}$ of the electron ($\xi = e$) or phonon ($\xi = p$) gases in the matrix material are given by

$$k_{\xi,m} = \frac{K_{\xi,m}}{1 + l_{\xi\xi,m}\sigma_\perp f}, \tag{3.5}$$

where $K_{\xi,m}$ is the bulk thermal conductivity of the matrix given by (3.2) with the replacement $l_\xi \to l_{\xi\xi,m}$, which, for the sake of simplicity, has been represented by its average value. Equation (3.5) indicates that the size dependence of the effective thermal conductivity $k_{\xi,m}$ of the matrix is related by the collision cross-section per unit volume ($\sigma_\perp = A_\perp/V$) and not through the total surface area per unit volume of the particles, as was suggested by other researchers [15, 21].

The effective thermal conductivity of the particles can be found similarly. Based on the Matthiessen rule, the effective mean free path $l_{\xi,I}$ of the energy carriers within the particles is given by

$$\frac{1}{l_{\xi,I}} = \frac{1}{l_{\xi\xi,I}} + \frac{1}{c}. \tag{3.6}$$

where c is the average distance traveled by the energy carriers inside the particles, independently of the intrinsic carrier scattering associated with the MFP $l_{\xi\xi,I}$. After replacing (3.6) into (3.2) and assuming that $l_{\xi\xi,I}$ can be represented by its average value, the following thermal conductivity $k_{\xi,I}$ of the particles is obtained

$$k_{\xi,I} = \frac{K_{\xi,I}}{1 + l_{\xi\xi,I}/c}, \tag{3.7}$$

where $K_{\xi,I}$ is the bulk thermal conductivity of the particles, defined by (3.2) with the replacement $l_\xi \to l_{\xi\xi,I}$. Equation (3.7) shows that the effective thermal conductivity of the particles can be considerably smaller than its bulk value when $c \leq l_{\xi\xi,I}$, and it

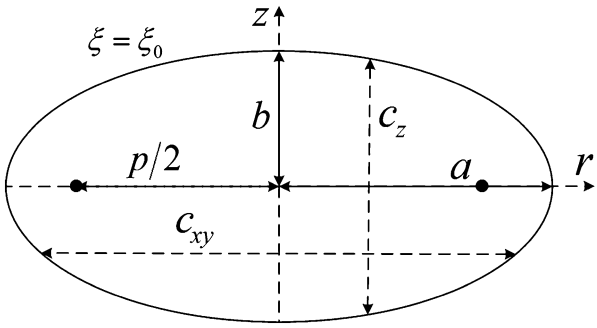

Fig. 3.5 Geometry of the cross-section of an oblate spheroid ($a > b$) with $r^2 = x^2 + y^2$

reduces to its bulk counterpart for $c \gg l_{\xi\xi,I}$. This is expected given that the distance c is directly proportional to the size of the particles, as shown below.

If the particles are aligned spheroids as the one shown in Fig. 3.4b, and the heat flux is in the z-direction (the resultant net direction of the energy carriers), the energy carriers of the matrix "see" an effective area of collision $A_\perp = \pi a^2$, which implies that $\sigma_\perp = \pi a^2/(4\pi b a^2/3) = 3/4b$. Due to the symmetry of the problem, the characteristic length $c = c_z$, can be calculated conveniently using prolate (if $a < b$) or oblate (if $a > b$) spheroidal coordinates (η, ξ, ϕ) [25]. The oblate spheroidal coordinates are related to the Cartesian coordinates (x, y, z) as follows

$$x = \frac{p}{2}\sqrt{(1-\eta^2)(1+\xi^2)}\cos\phi, \tag{3.8a}$$

$$y = \frac{p}{2}\sqrt{(1-\eta^2)(1+\xi^2)}\sin\phi, \tag{3.8b}$$

$$z = \frac{p}{2}\eta\xi, \tag{3.8c}$$

where p is the interfocal distance, as shown in Fig. 3.5. These oblate spheroidal coordinates are defined within the intervals $0 \leq \xi < \infty$, $-1 \leq \eta \leq 1$, and $0 \leq \phi < 2\pi$, such that the surface of the spheroid is defined by $\xi = \text{contant} = \xi_0$, the plane xy and the z axis are given by $\eta = 0$ and $|\eta| = 1$, respectively [25]. According to these definitions and (3.8a)–(3.8c), the lengths of the axes of the spheroid are determined by $2a = p\sqrt{1+\xi_0^2}$ and $2b = p\xi_0$.

To calculate the mean distance c, we are going to assume that the energy carriers undergo diffusive scattering at the inner surface of the spheroidal particles. This means that the electrons and phonons are reflected from the boundary surfaces with equal probability to any direction, as is the case of rough interfaces, which are usually found in practical applications. In presence of a heat flux along the z axis the distance $c = c_z$, is therefore determined by the average value of $2z_0 = p\eta\xi_0$ (see Fig. 3.5), that is to say

$$c_z = \frac{p\xi_0}{A}\int_A \eta dA, \tag{3.9}$$

where, according to (3.8a)–(3.8c), the differential element of area over the surface of the spheroid is given by $dA = (p/2)^2\sqrt{1+\xi^2}\sqrt{\eta^2+\xi^2}d\eta d\phi$. The integration in (3.9) has to be performed over the total area A of the spheroid, and its result is

$$c_z = \frac{4b}{3\varepsilon}\frac{\sqrt{1+\varepsilon^2}^3 - 1}{\varepsilon\sqrt{1+\varepsilon^2}+\text{arcsinh}(\varepsilon)}, \tag{3.10}$$

where $\varepsilon = \sqrt{(a/b)^2-1}$ is the eccentricity of the oblate spheroids. For spherical particles, the characteristic length in (3.10) reduces to the radius of the spheres ($c_z = b = a$), which is consistent with its definition of mean distance. On the other hand, for flat-plate particles ($a \gg b$), (3.10) becomes $c_z = 4b/3 \approx 1.33b$. According to (3.7), this indicates that the thinner the particle, the smaller its thermal conductivity across its plane, as expected.

If the heat flux is parallel to the xy-plane, the cross-section is given by $A_\perp = \pi ab$ and hence $\sigma_\perp = \pi ab/(4\pi ba^2/3) = 3/4a$. Furthermore, according to Fig. 3.4, the distance $c = c_{xy}$ traveled by the energy carriers inside the oblate spheroids is given the average value of $2y_0 = p\sqrt{(1-\eta^2)(1+\xi_0^2)}\sin\phi$, over the surface of the spheroid. The final results is

$$c_{xy} = \frac{8a}{3\pi\varepsilon}\frac{(1+\varepsilon^2)D(-\varepsilon^2) - (1-\varepsilon^2)E(-\varepsilon^2)}{\varepsilon\sqrt{1+\varepsilon^2}+\text{arcsinh}(\varepsilon)}, \tag{3.11}$$

where D and E are the complete elliptic integrals of the first and second kind [26], respectively. For spherical particles, (3.8b) predicts $c_{xy} = b = a$, which agrees with (3.10). On the other hand, for flat-plate particles (3.11) yields $c_{xy} = 8a/3\pi \approx 0.85a$, which is independent of the minor semi-axis and increases linearly with the major semi-axis of the spheroid. By comparing the values $c_z = 1.33b$ and $c_{xy} = 0.85a$, for a flat-plate particle ($a \gg b$), it is clear that its thermal conductivity along its plane is much larger than the one across its plane (see (3.7)).

By using the prolate spheroidal coordinates and following a similar procedure than the one performed for oblate spheroids, a direct calculation shows that for prolate spheroids ($a < b$), (3.10) and (3.11) remains valid after the substitution $\varepsilon \to i\varepsilon$, where $i = \sqrt{-1}$ is the imaginary unit and the new eccentricity is $\varepsilon = \sqrt{1-(a/b)^2}$. Therefore, for cylindrical inclusions ($a \ll b$), (3.10) and (3.11) reduces to $c_z = 8b/3\pi \approx 0.85b$ and $c_{xy} = 32a/3\pi^2 \approx 1.08a$, which indicate that the thermal conductivity along the axis of the particles can be much larger than the one across its axis, as is the case of carbon nanotubes [27], for instance. Figure 3.6a shows that for a fixed semi-axis b, the characteristic

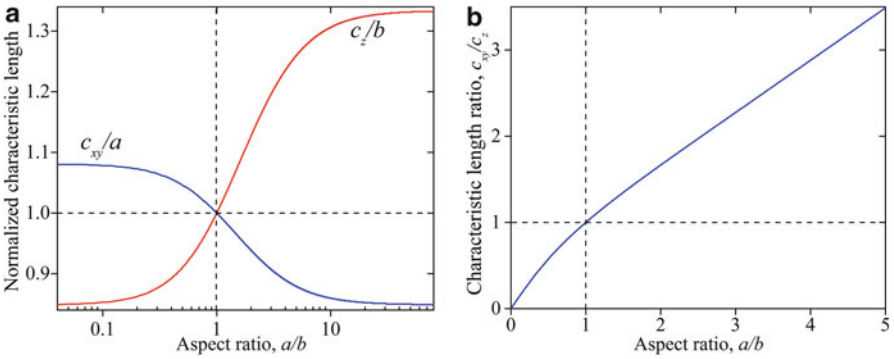

Fig. 3.6 (**a**) Normalized characteristic lengths and (**b**) characteristic length ratio c_{xy}/c_z as a function of the aspect ratio a/b of spheroidal particles

length c_z is bounded and increases with the equatorial radius a of the spheroids. On the other hand, for a given semi-axis a, the characteristic length c_{xy} is also bounded and increases with b. These behaviors are because of the average distance that the energy carriers can travel inside the particles increases with their dimensions. This is confirmed by Fig. 3.6b, which indicates that for prolate spheroids ($a < b$), $c_{xy} < c_z$; while for oblate ones ($a > b$), $c_{xy} > c_z$; as expected.

By replacing the bulk thermal conductivities $K_{\xi,m}$ and $K_{\xi,I}$ involved in a Fourier-law-based model for the thermal conductivity of composites with a defined distribution of particles, with their corresponding modified values given by (3.5) and (3.7), it is expected that the its validity can be extended for composites with nano-sized particles, as is the case of nanocomposites. Given that the modified thermal conductivities are smaller than their corresponding bulk values, it is expected that the modified thermal conductivity of the whole composite is smaller than its unmodified value.

3.2.2 *Applications*

Now let us consider a composite made up of aligned Si particles embedded in a Ge matrix, where the main heat carriers are the phonons. A suitable model for this case, was derived by Nan et al. [8], who proposed that the components k_i of the thermal conductivity of the composite, along the principal axes ($i = x, z$) of the aligned spheroidal particles are given by

$$k_i = K_m \frac{1 + \beta_i (1 - L_i) f}{1 - \beta_i L_i f}, \tag{3.12}$$

where K_m is the bulk thermal conductivity of the matrix, $2L_x + L_z = 1$, and

$$\beta_i = \frac{\sigma_i - K_m}{K_m + L_i(\sigma_i - K_m)}, \tag{3.13a}$$

$$\sigma_i = \frac{K_I}{1 + RL_iK_I(2/a + 1/b)}, \tag{3.13b}$$

$$L_x = \frac{p^2}{2(p^2-1)} - \frac{p}{2\sqrt{p^2-1}^3}\text{arccosh}(p), \tag{3.13c}$$

where K_I the thermal conductivity of the inclusions, R the interfacial thermal resistance and $p = b/a$. According to (3.5) and (3.7), the modified thermal conductivity of the inclusions and the matrix are $k_I = K_I/(1 + l_{pp,I}/c)$ and $k_m = K_m/(1 + 3l_{pp,m}f/4d)$, respectively; where $d = a$ (b) for oblate (prolate) spheroids. After replacing these two results into (3.12), (3.13a) and (3.13b), the modified EMA model is obtained.

Figure 3.7a shows the thermal conductivity $k = k_x = k_z$ of the nanocomposite as a function of the volume fraction f for different values of the radius $a = b$ of spherical particles, in comparison with numerical results obtained from the Boltzmann transport equation [13, 15, 21]. Here, the cubic particles studied numerically [21] are represented approximately by spherical particles. The calculations were performed using the data shown in Table 3.1, for the modified (M) and unmodified (UM) models.

Note that the predictions of the modified model are in good agreement with the MC simulations, especially for $a = 5$ and 25 nm, which are much smaller than the phonon MFP, and therefore the interfacial scattering plays an important role. A similar behavior is shown in Fig. 3.7b, for the thermal conductivity of composites in the direction perpendicular to the aligned cylindrical particles ($a \ll$ b), where the predictions of the modified model again agree with the numerical results based on the BTE. A remarkable disagreement between the predictions of the modified and unmodified models is shown in Fig. 3.7a, b, for both spherical and cylindrical particles, respectively. As the size of the particles increases ($a = 100$ nm) and becomes of the same order of magnitude than the MFP, this difference decreases, as a consequence of the reduction of the boundary scattering of phonons.

Furthermore, the modified EMA model can also be used to predict anisotropic thermal conductivity of nanocomposites with spheroidal particles. Figure 3.8a, b show the anisotropic thermal conductivities k_x and k_z of nanocomposites as a function of the volume fraction for three different particles sizes of $a = 5$, 50, 300 nm and $b = 5a$.

Figure 3.8a shows that k_x has a similar decreasing trend than the one for spherical particles shown in Fig. 3.7a. By contrast, Fig. 3.8b shows that the thermal conductivity of the composite can also increase with the volume fraction for $a = 300$ nm. According to (3.12), the increasing (decreasing) of the composite thermal conductivity when the volume fraction increases is determined by $\beta > 0$ $(\beta < 0)$. Based on this remark and according to (3.13a) and (3.13b), the thermal conductivity of a composite will decrease independently of the value of the thermal conductivity of

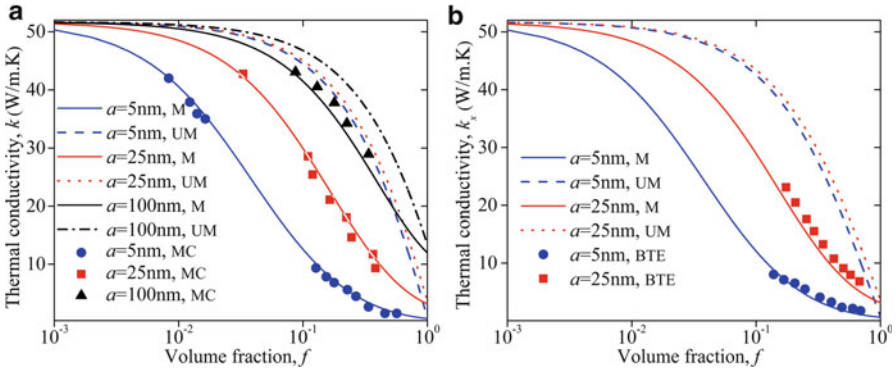

Fig. 3.7 Thermal conductivity of a Si/Ge nanocomposite reinforced with (**a**) spherical and (**b**) cylindrical nanoparticles, as a function of the volume fraction and the particle radius. Calculations were performed with the data reported in Table 3.1

Table 3.1 Material properties used in the calculations [21]

Material	Bulk thermal conductivity (W/mK)	MFP (nm)	Interfacial thermal resistance (m^2K/W)
Si	150	268	6.8×10^{-9}
Ge	51.7	171	

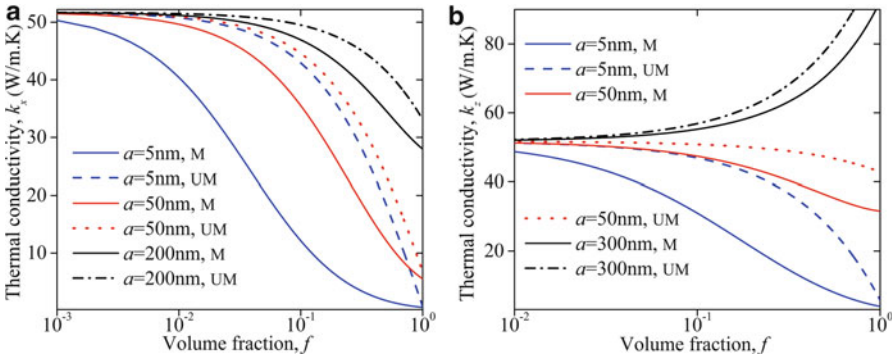

Fig. 3.8 Thermal conductivities (**a**) k_x and (**b**) k_z of a Si/Ge nanocomposite reinforced with prolate spheroids with semi-axes $b = 5a$. Calculations were performed with the data reported in Table 3.1

the particles, when the volume fraction of the particles increases, if the geometry of the particles fulfills the condition

$$\left(\frac{2}{a}+\frac{1}{b}\right)L_i > \frac{1}{a_K}, \tag{3.14}$$

where $a_K = RK_m$ is the so-called Kapitza radius of the composite. Equation (3.14) represents the selection rule to minimize the thermal conductivity of composite

materials by arranging the size and shape of the spheroidal particles properly. For spherical and cylindrical particles of radius a, (3.14) reduces to $a_K > a$, which agrees with the results shown in Fig. 3.7a, b.

3.3 Metal-Nonmetal Composites

In metal-nonmetal composites, heat is conducted by different carriers in the particles and in the matrix. The energy is transport by both electrons and phonons in metallic particles and then coupled to the phonons in the matrix. Both the electron–phonon coupling in the metallic particle and the energy coupling across material interface become important factors that determines the thermal conductivity of composites, especially when the particle size is in the order of the electron–phonon coupling length. In this section, the two-temperature model of heat conduction [28] originally proposed by Kaganov et al. [29] and Anisimov et al. [30] is used to take into account the electron–phonon interactions and to determine the effective thermal conductivity of composites with spheroidal metallic particles embedded in a nonmetallic matrix. The interfacial thermal resistance that accounts for the phonon mismatch between the two phases is included in this model. Our results generalize those obtained by Nan et al. [8] under the framework of the Fourier law of heat conduction and show that the effective thermal conductivity depends strongly on (1) the relative size of the spheroidal particles with respect to the electron–phonon coupling length, and (2) the ratio between the electron and phonon thermal conductivities. It is shown that the composite thermal conductivity has upper and lower bounds, which are determined by the particle size in comparison with the electron–phonon coupling length. For the limiting case of perfect electron–phonon coupling, the proposed model reduces to various previously reported results. This study could be useful for guiding the design of particulate composites with metallic inclusions from macro/micro- to nano-scales.

3.3.1 Theoretical Model

Figure 3.9a shows the particulate composite under consideration, in which coated spheroidal particles with the orientation and geometry shown in Fig. 3.9b are embedded in a dielectric matrix of thermal conductivity k_3. The metallic core of the spheroidal particles has electron and phonon thermal conductivities k_e and k_p respectively, and it is covered by a dielectric layer of thermal conductivity k_2 with variable thickness. Note that the composite shown in Fig. 3.9a, b is a three-phase composite, which can be used to model two-phase composite when the thickness of the dielectric coating goes to zero and the coating is used to represent a finite interfacial thermal resistance. The derivation of the effective thermal conductivity of this composite will be based on finding the temperature profile outside the

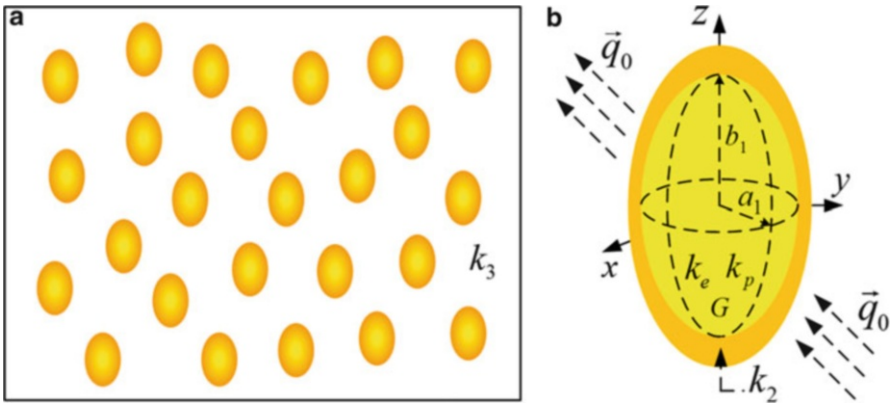

Fig. 3.9 Schematics of (**a**) the composite with aligned coated spheroidal particles and, (**b**) the geometry of one of those particles made of a metallic core with electron thermal conductivity k_e, phonon thermal conductivity k_p and electron–phonon coupling factor G; and a nonmetallic coating layer with thermal conductivity k_2. The semi axes a_2 and b_2 of the outer confocal spheroid satisfy the relation $a_2^2 - b_2^2 = a_1^2 - b_1^2$

particle shown in Fig. 3.9b, when it is exposed to a constant heat flux $\vec{q}_0$. This method is based on the approach developed by Maxwell for an analogous electrostatics problem [3].

In the metallic core, the TTM of heat conduction is used to describe the coupled heat transport due to the electron and phonon gases [31]. This model describes the spatial evolution of electron temperature T_e and the phonon temperature T_p by the following coupled differential equations [28, 31]

$$\nabla^2 T_e - \frac{G}{k_e}\left(T_e - T_p\right) = 0, \tag{3.15a}$$

$$\nabla^2 T_p + \frac{G}{k_p}\left(T_e - T_p\right) = 0, \tag{3.15b}$$

where G is the electron–phonon coupling factor, which takes into account the electron–phonon interactions. Note that if the electron gas is in thermal equilibrium with the phonon gas ($T_e = T_p$), both (3.15a) and (3.15b) reduces to the Laplace equation, which indicates that the difference between TTM and the Fourier law is due to the non-equilibrium state between electrons and phonons inside the metallic particles. According to (3.15a) and (3.15b), the thermal equilibrium between electrons and phonons is reached when $G \to \infty$ (perfect coupling), which indicates that in this limit, the predictions of the current approach should reduce to the results obtained under the Fourier law, as shown below.

We point out that the electron–phonon coupling G in nanostructures is temperature-dependent and could be remarkably different from that in the bulk materials [32–34]. However, many reported results have shown that the predictions

of the TTM with an average constant value of G are in good agreement with experimental data [31–33]. Based on these results and with the objective of keeping solvable the problem, we are going to consider that the coupling factor can be represented by an average constant value to illustrate the importance of G in modeling the thermal conductivity of composites. Phonons dominate the heat conduction in the nonmetallic coating layer and in the matrix and therefore the Fourier law of heat conduction can describe their temperature.

By subtracting (3.15a) and (3.15b), the electron and phonon temperature difference $\psi = T_e - T_p$ can be found by

$$\nabla^2\psi - \frac{1}{d^2}\psi = 0, \tag{3.16}$$

where d is the electron–phonon coupling length of metals defined by

$$d^2 = \frac{k_a}{G}, \tag{3.17a}$$

$$\frac{1}{k_a} = \frac{1}{k_e} + \frac{1}{k_p}, \tag{3.17b}$$

where k_a is the half of the harmonic mean of the electron and phonon thermal conductivities. It was found that $d \sim 10^{-7}$ m, for a wide variety of metals (as copper, silver, gold and others) at room temperature [28, 31].

Due to the symmetry of the problem, we can use the prolate ($b_1 > a_1$) or oblate ($b_1 < a_1$) spheroidal coordinates (η, ξ, ϕ) to simplify the solution of the problem. Let us now first consider that the uniform heat flux $\vec{q}_0$ shown in Fig. 3.9b is applied in the z-direction. Then, based on the Fourier law and in the relations among the oblate spheroidal coordinates with the Cartesian coordinates defined in (3.8a)–(3.8c), the temperature T_3 far away from the influence of the coated particle, apart from an additive constant, is given by

$$T_3(|z| \to \infty) \equiv T_0 = -\frac{q_0}{k_3}z = -\frac{q_0 p}{2k_3}\eta\xi, \tag{3.18}$$

Taking into account the azimuthal symmetry of the problem, the method of separation of variables indicates that the difference of the electron and phonon temperature can be written as $\psi(\eta,\xi) = S(\eta)R(\xi)$. After replacing this expression into (3.16), it is found that the functions $S(\eta)$ and $R(\xi)$ satisfy the following differential equations

$$\frac{d}{d\eta}\left[\left(1-\eta^2\right)\frac{dS}{d\eta}\right] + \left(\lambda - c^2\eta^2\right)S = 0, \tag{3.19a}$$

$$\frac{d}{d\xi}\left[\left(1+\xi^2\right)\frac{dR}{d\xi}\right]-\left(\lambda+c^2\xi^2\right)R=0, \tag{3.19b}$$

where λ is a separation constant and $c = p/(2d)$. Note that for $c = 0$ ($d = \infty$), the well-behaved solution of (3.19a) and (3.19b) can be expressed in terms of the first and second Legendre polynomials P_l and Q_l, respectively [26]. In this case ($c = 0$), (3.16) reduces to the Laplace equation and therefore it yields the solution for the temperature T under the Fourier law description. Taking into account that $Q_l(\mu) \propto P_l(\mu)F_l(\mu)$ [35], the general solution for T, can be written as follows

$$T(\eta,\xi)=\sum_{l=0}^{\infty}A_lP_l(\eta)P_l(i\xi)[1+B_lF_l(i\xi)], \tag{3.20}$$

where A_l and B_l are constant that depend on the boundary condition of the problem, i is the imaginary unit, and

$$F_l(\mu)=\int_{\mu}^{\infty}\frac{dx}{(x^2-1)[P_l(x)]^2}. \tag{3.21}$$

The temperature profile in the nonmetallic coating layer T_2, and in the matrix T_3, can be therefore written as (3.20), which is a particular case ($c = 0$) of the general solution of (3.19a) and (3.19b).

For the case of $c \neq 0$ ($d \neq \infty$) the solution of (3.19a) is determined by the spheroidal angular functions $S = S_{0l}(c,\eta)$, which are similar to the well-known spherical harmonics and can be expanded in term of Legendre polynomials [25]. Analogously, the solution of (3.19b) is given by the spheroidal radial functions $R = R_{0l}(c,i\xi)$, which have a known expansion in terms of spherical Bessel functions [25]. We can therefore write the general solution of (3.16) as follows

$$\psi(\eta,\xi)=\sum_{l=0}^{\infty}C_lS_{0l}(c,\eta)R_{0l}(c,i\xi), \tag{3.22}$$

where C_l are numerical constants. According to (3.15a), the electron temperature T_e satisfies

$$\nabla^2T_e=\frac{G}{k_e}\psi, \tag{3.23}$$

which is an inhomogeneous partial differential equation, whose general solution is given by the superposition of its complementary (T_{ec}) and particular (T_{ep}) solutions ($T_e = T_{ec} + T_{ep}$) [26]. Taking into account that $\nabla^2T_{ec} = 0$, the solution for T_{ec} is given by (3.20). Furthermore, the combination of $\nabla^2T_{ep} = \psi G/k_e$ with (3.16) yields $T_{ep} = \psi k_a/k_e$. In this way, the general solution of (3.23) is

$$T_e(\eta,\xi) = T(\eta,\xi) + \frac{k_a}{k_e}\psi(\eta,\xi). \tag{3.24}$$

The phonon temperature $T_p = T_e - \psi$ is then found to be

$$T_p(\eta,\xi) = T(\eta,\xi) - \frac{k_a}{k_p}\psi(\eta,\xi). \tag{3.25}$$

Note that (3.24) and (3.25) shows that the temperature profiles predicted by the TTM are given by the superposition of the Fourier law prediction (the common term) and a non-equilibrium term, which takes into account the effects of the coupling among the electrons and phonons of the metallic core of the particle shown in Fig. 3.9b.

After writing out the solutions for temperature distributions inside the particle [(3.24) and (3.25)], in the coating layer and in the matrix [(3.20)], we now need to specify interface and boundary conditions to find the required specific solutions. In general, there are two possible pathways for energy transport across metal-nonmetal interfaces, namely: (1) coupling between electrons and phonons within the metal, and then subsequently coupling between phonons of the metal and phonons of the nonmetal, and (2) coupling between electrons of the metal and phonons of the nonmetal through anharmonic interactions at the metal–nonmetal interfaces.

Even though the direct electron–phonon coupling at metal-nonmetal interfaces is always present (pathway 2), experimental or theoretical methodologies to quantify its contribution are scarce [28, 36]. The description of this channel of heat transport is complicated, and the mechanism is not well understood, especially when the electrons of the metal are not in equilibrium with the phonons of the dielectric material [37, 38]. The authors of these latter works also suggested that contribution of the pathway 2 to the total heat flux through the metal-dielectric interface could be small in comparison to that of the phonon-phonon interactions for a wide variety of metals. Based on these facts and for keeping the problem analytically solvable, we only consider the pathway 1 in this chapter.

Given that the metallic particles are embedded in a nonmetallic matrix, it is reasonable to consider that the electrons are mainly isolated inside the particles. We therefore assume that the electrons inside the core particle do not interact directly with phonons in nonmetals and focus our study on the effect of electron–phonon coupling on the effective thermal conductivity of the composite. Under this condition, the boundary conditions for the temperature and heat flux continuity at the interfaces, can be written as

$$\left.\frac{\partial T_e}{\partial \xi}\right|_{\xi=\xi_1} = 0, \tag{3.26a}$$

$$T_p\big|_{\xi=\xi_1} = T_2\big|_{\xi=\xi_1}, \tag{3.26b}$$

$$k_p \left.\frac{\partial T_p}{\partial \xi}\right|_{\xi=\xi_1} = k_2 \left.\frac{\partial T_2}{\partial \xi}\right|_{\xi=\xi_1}, \tag{3.26c}$$

$$T_2|_{\xi=\xi_2} = T_3|_{\xi=\xi_2}, \tag{3.26d}$$

$$k_2 \left.\frac{\partial T_p}{\partial \xi}\right|_{\xi=\xi_2} = k_3 \left.\frac{\partial T_3}{\partial \xi}\right|_{\xi=\xi_2}, \tag{3.26e}$$

where ξ_1 and ξ_2 represent the surfaces of the inner and outer spheroids, respectively. The boundary conditions expressed in (3.18) and (3.26a)–(3.26e) determine the temperature profiles everywhere in the space. An enormous amount of algebraic calculations can be saved during the evaluation of these boundary conditions, by recognizing that the general form of the temperature profiles is dictated by the form of the external thermal excitation [39]. Given that (3.18) has a linear dependence on η, the response of the materials should also have the same dependence, which implies that $l = 1$ in (3.20) and (3.22). Therefore (3.20), (3.24) and (3.25) can be written as

$$T_e(\eta, \xi) = AT_0(\eta, \xi)\left[1 + B\frac{k_a}{k_e}\frac{i_1(c\xi)}{\xi}\right], \tag{3.27a}$$

$$T_p(\eta, \xi) = AT_0(\eta, \xi)\left[1 - B\frac{k_a}{k_p}\frac{i_1(c\xi)}{\xi}\right], \tag{3.27b}$$

$$T_2(\eta, \xi) = CT_0(\eta, \xi)[1 + DF(\xi)], \tag{3.27c}$$

$$T_3(\eta, \xi) = T_0(\eta, \xi)[1 + EF(\xi)], \tag{3.27d}$$

where T_0 is defined by (3.18), $F(\xi) = iF_1(i\xi)$, $i_1()$ is the modified spherical Bessel function of the first kind and order one, and A, B, C, D and E are constants, which are determined by substituting (3.27a)–(3.27d) into the five boundary conditions given in (3.26a)–(3.26e). For the purposes of this work, just the temperature T_3 outside of the spheroid is required and its explicit expression is

$$T_3(\eta, \xi) = T_0(\eta, \xi)\left[1 + \beta_{33}\frac{F(\xi)}{\xi_2 F'(\xi_2)}\right] = T_0(\eta, \xi)\left[1 - \beta_{33}L_{33}^{(2)}\frac{F(\xi)}{F(\xi_2)}\right], \tag{3.28}$$

where the prime ($'$) indicates derivative of F with respect to its argument, and

$$\beta_{33} = \frac{k_{33} - k_3}{k_3 + (k_{33} - k_3)L_{33}^{(2)}}, \tag{3.29a}$$

$$\frac{k_{33}}{k_2} = \frac{1 + \alpha_{33}\left(1 - L_{33}^{(2)}\right)\nu}{1 - \alpha_{33}L_{33}^{(2)}\nu}, \tag{3.29b}$$

$$\alpha_{33} = \frac{k_1 - k_2}{k_2 + (k_1 - k_2)L_{33}^{(1)}}, \tag{3.29c}$$

$$k_1 = \frac{k_e + k_p}{\chi}, \tag{3.29d}$$

$$\chi = 1 + \frac{k_e}{k_p}\frac{d}{b_1}\frac{i_1(b_1/d)}{i'_1(b_1/d)}, \tag{3.29f}$$

$$L_{33}^{(j)} = \left(1 + e_l^{-2}\right)\left(1 - \frac{\arctan(e_j)}{e_j}\right), \tag{3.29g}$$

where $\nu = a_1^2 b_1/a_2^2 b_2$ is the volume fraction of the core spheroid relative to the total volume of the coated particle, $e_j = \sqrt{(a_j/b_j)^2 - 1}$ is the eccentricity of the $j = 1, 2$ oblate spheroid ($a_j > b_j$) and all other parameters have been defined before. In deriving (3.29a)–(3.29g), the relations $a_j = (p_j/2)\sqrt{1 + \xi_j^2}$ and $b_j = p_j\xi_j/2$ have been used [25]. It is worthwhile to point out the following remarks on (3.29a)–(3.29g): (1) In absence of the coating layer ($\nu = 1$) and without considering the interfacial thermal resistance, the thermal conductivity k_{33} reduces to the thermal conductivity of the inner spheroid ($k_{33} = k_1$). This indicates that in presence of the coating layer, the thermal conductivity k_{33} can be considered as the effective thermal conductivity of the coated spheroidal particle. (2) The effect of the electron–phonon coupling appears in the parameter χ through the ratio between the minor semi-axis of the inner spheroid and the coupling length d defined in (3.17a). Thus, the relative size of the particles with respect to the coupling length plays an important role in the process of heat conduction. (3) Equation (3.29g) defines the well-known geometrical factor [39], along the minor z axis of the oblate spheroids.

The effective thermal conductivity of the composite can be derived using the temperature profile given by (3.28). To do that, let us consider a large spheroid with semi-axes a_0 and b_0, and surface $\xi = \xi_0$, composed by N aligned small spheroids (see Fig. 3.9a), with the geometry and thermal conductivities shown in Fig. 3.9b, embedded in a matrix of thermal conductivity k_3. Assuming that the volume fraction of the N spheroids $f = Na_2^2 b_2/a_0^2 b_0$ is small enough to neglect the interaction among them (dilute limit), at distances much larger than the major semi-axis a_0, the heat flux (and therefore the temperature) is simply the superposition of the heat fluxes due to each small spheroid. Under this condition, (3.28) indicates that the temperature profile due to the system of N particles can be written as follows

$$T_3(\eta, \xi) = T_0(\eta, \xi)\left[1 + N\beta_{33}\frac{F(\xi)}{\xi_2 F'(\xi_2)}\right]. \tag{3.30a}$$

By considering the large spheroid as a homogeneous spheroid with effective thermal conductivity K_{33} along its minor axis (z-direction), the temperature profile generated at a large distance is

$$T_3(\eta,\xi) = T_0(\eta,\xi)\left[1+\beta_{33}^{*}\frac{F(\xi)}{\xi_0 F^{'}(\xi_0)}\right], \tag{3.30b}$$

where β_{33}^{*} is defined by (3.29a) with the replacement $k_{33} \to K_{33}$. After equating (3.30a) with (3.30b), it is found that $\beta_{33}^{*} = \beta_{33} f$, where $f = N\xi_0 F'(\xi_0)/\xi_2 F'(\xi_2)$ is the volume fraction of the N particles. The solution of the former equation for K_{33} yields

$$\frac{K_{33}}{k_3} = \frac{1+\beta_{33}\left(1-L_{33}^{(2)}\right)f}{1-\beta_{33}L_{33}^{(2)}f}. \tag{3.31}$$

Note that (3.31) has a similar mathematical form as (3.29b), which indicates that the effective thermal conductivities of the composite and the coated particles are determined by the same mathematical equation with different physical parameters.

So far, the calculations have been performed considering that the applied heat flux $\vec{q}_0$ is along the z axis of the aligned oblate spheroidal inclusions. When this heat flux is parallel to the x or y axis, we can follow a similar procedure to find the effective thermal conductivities K_{11} and K_{22}, along the x and y axes, respectively. Indeed we find that $K_{11} = K_{22}$, as expected; due to the symmetry of the coated spheroids and they are given by (3.31) with the replacement of the all subscripts $33 \to 11$, while the geometrical factors $L_{11}^{(j)}$ satisfy the relation

$$2L_{11}^{(j)} + L_{33}^{(j)} = 1, \tag{3.32}$$

which implies that none of the (positive) geometrical factors of the spheroidal particles is larger than the unity.

If the particles are prolate coated spheroids ($b_1 > a_1$), we can derive the effective thermal conductivities $K_{11} = K_{22}$ and K_{33} of the anisotropic composite along the principal axes of the aligned spheroids using the prolate spheroidal coordinates [25] and following a similar procedure as that we have performed for the oblate spheroids. The results are indeed still given by equations of the form of (3.31), with minor changes on the geometrical terms defined in (3.29f) and (3.29g) that are specified below.

In summary, the effective thermal conductivities of the particulate composite along the principal axes of the aligned oblate or prolate coated spheroids can be written as follows

$$\frac{K_{ii}}{k_3} = \frac{1+\beta_{ii}\left(1-L_{ii}^{(2)}\right)f}{1-\beta_{ii}L_{ii}^{(2)}f}, \tag{3.33a}$$

$$\beta_{ii} = \frac{k_{ii} - k_3}{k_3 + (k_{ii} - k_3)L_{ii}^{(2)}}, \tag{3.33b}$$

$$\frac{k_{ii}}{k_2} = \frac{1 + \alpha_{ii}\left(1 - L_{ii}^{(2)}\right)\nu}{1 - \alpha_{ii}L_{ii}^{(2)}\nu}, \tag{3.33c}$$

$$\alpha_{ii} = \frac{k_1 - k_2}{k_2 + (k_1 - k_2)L_{ii}^{(1)}}, \tag{3.33d}$$

$$k_1 = \frac{k_e + k_p}{\chi}, \tag{3.33e}$$

$$\chi = 1 + \frac{k_e}{k_p}\begin{cases} \dfrac{d}{b_1}\dfrac{i_1(b_1/d)}{i_1'(b_1/d)}, & \text{Oblate spheroids} \\ \dfrac{d}{a_1}\dfrac{i_1(a_1/d)}{i_1'(a_1/d)}, & \text{Prolate spheroids} \end{cases} \tag{3.33f}$$

$$L_{33}^{(j)} = \begin{cases} \left(1 + e_j^{-2}\right)\left(1 - \dfrac{\arctan(e_j)}{e_j}\right), & \text{Oblate spheroids} \\ \left(1 - e_j^{-2}\right)\left(1 - \dfrac{\arctan\ h(e_j)}{e_j}\right), & \text{Prolate spheroids} \end{cases} \tag{3.33g}$$

where $e_j = \sqrt{\left(a_j/b_j\right)^2 - 1}$ for oblate spheroids and $e_j = \sqrt{1 - \left(a_j/b_j\right)^2}$ for prolate spheroids, and the prime ($'$) indicates derivative of $i_1()$ with respect to its argument. It is important to note that as a result of the electron–phonon interactions at the metallic particle, its total thermal conductivity (electron + phonon contributions) is reduced by the factor χ, which can be much larger than the unity when the size of the particles is of the same order of magnitude than the coupling length, as established in (3.33f). This reduction is reasonable, given that these interactions represent a scattering process between the electrons and phonons, which reduces their total mean free path and therefore the corresponding thermal conductivity [24, 40].

When the applied heat flux $\vec{q}_0$ is not parallel to any of the principal axes of the coated spheroids, we can generalize (3.33a)–(3.33g). In this case, the heat flux $\vec{q}_3$ due to the temperature T_3 outside of the spheroids is determined by the principle of superposition and can be written as follows

$$\vec{q}_3 = -k_3\left(\hat{x}\left.\frac{\partial T_3}{\partial x}\right|_{\beta_{11},q_{0,11}} + \hat{y}\left.\frac{\partial T_3}{\partial y}\right|_{\beta_{22},q_{0,22}} + \hat{z}\left.\frac{\partial T_3}{\partial z}\right|_{\beta_{33},q_{0,33}}\right), \tag{3.34}$$

where $q_{0,ii}$ for $i = 1, 2, 3$ are the components of $\vec{q}_0$ relative to the coordinate system (x, y, z) defined as the principal axes of the coated spheroids, and T_3 is given by (3.28), for the appropriate parameters specified as subscripts. The components of the heat flux vector $\vec{q}_3$ relative to the (x',y',z') coordinate system, where the applied heat flux vector $\vec{q}_0$ is parallel to the z' axis (for example), can be obtained with the equation $\left(\vec{q}_3\right)' = M\left(\vec{q}_3\right)$, where M is the transformation matrix and the parenthesis indicate that the heat flux vector is written in matrix form [41]. Note that this latter equation represents the way in which the coordinates of any vector transform from its original coordinate system to a rotated one. This relation together with (3.34) implies that the parameters β_{ii} and $\beta_{ii}L_{ii}^{(2)}$ (see (3.28)) transform according to [41]

$$(\beta)' = M(\beta)M^{-1}, \tag{3.35a}$$

$$\left(\beta L^{(2)}\right)' = M\left(\beta L^{(2)}\right)M^{-1}, \tag{3.35b}$$

where

$$(\beta) = \begin{pmatrix} \beta_{11} & 0 & 0 \\ 0 & \beta_{11} & 0 \\ 0 & 0 & \beta_{33} \end{pmatrix}, \tag{3.36a}$$

$$\left(\beta L^{(2)}\right) = \begin{pmatrix} \beta_{11}L_{11}^{(2)} & 0 & 0 \\ 0 & \beta_{11}L_{11}^{(2)} & 0 \\ 0 & 0 & \beta_{33}L_{33}^{(2)} \end{pmatrix}. \tag{3.36b}$$

Let us now consider that the z axis of the coated spheroids forms an angle θ with the direction of propagation of the applied heat flux (z' direction), as shown in Fig. 3.10. When the coated spheroids are randomly distributed in the plane $x'y'$, this angular displacement between the z and z' axes can be described by a single rotation along the x axis. Therefore the transformation matrix M takes the form [41]

$$M = \begin{pmatrix} 1 & 0 & 0 \\ 0 & \cos\theta & \sin\theta \\ 0 & -\sin\theta & \cos\theta \end{pmatrix}. \tag{3.37}$$

After inserting (3.36a), (3.36b) and (3.37) into (3.35a) and (3.35b), the parameters β'_{ii} and $(\beta L^{(2)})'_{ii}$ can be found. The substitution of these latter results into (3.33a) shows that the components of the effective thermal conductivity K_{ii}^* along the x', y' and z' axes (the laboratory coordinate system) are determined by

$$\frac{K_{11}^*}{k_3} = \frac{K_{22}^*}{k_3} = \frac{2 + \left[\beta_{11}\left(1 - L_{11}^{(2)}\right)(1+\gamma) + \beta_{33}\left(1 - L_{33}^{(2)}\right)(1-\gamma)\right]f}{2 - \left[\beta_{11}L_{11}^{(2)}(1+\gamma) + \beta_{33}L_{33}^{(2)}(1-\gamma)\right]f}, \tag{3.38a}$$

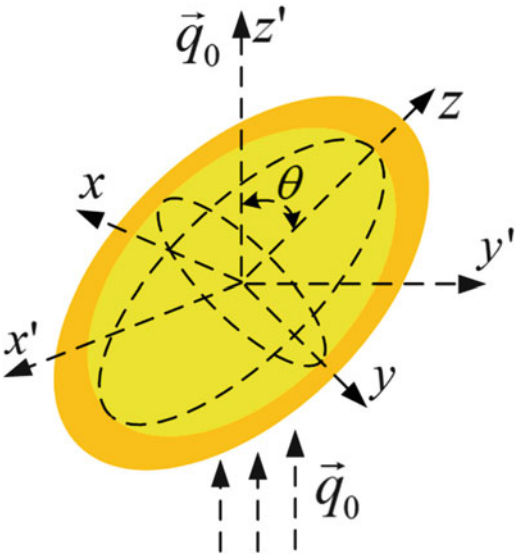

Fig. 3.10 Local (x, y, z) and global (x', y', z') coordinate systems of a coated spheroid

$$\frac{K_{33}^*}{k_3} = \frac{1 + \left[\beta_{11}\left(1 - L_{11}^{(2)}\right)(1-\gamma) + \beta_{33}\left(1 - L_{33}^{(2)}\right)\gamma\right]f}{1 - \left[\beta_{11}L_{11}^{(2)}(1-\gamma) + \beta_{33}L_{33}^{(2)}\gamma\right]f}, \tag{3.38b}$$

where $\gamma = \cos^2\theta$. Note that when $\theta = 0$ ($\gamma = 1$), (3.38a) and (3.38b) reduces to (3.33a), as expected. Equations (3.38a) and (3.38b) determine the effective thermal conductivity of particulate composites that are isotropic in the perpendicular directions to the applied heat flux and anisotropic under the heat flux direction. Thus, the obtained results involve the effects of the coupling length, size, shape, orientation and volume fraction of the particles.

We point out that the primary constituents of the composites under consideration are the matrix and the metallic particles, which are separated by a coating layer, as shown in Fig. 3.9b. This coating layer, as mentioned before, has been introduced to model the lack of thermal coupling at the interface between the matrix and metallic particles [42, 43]. Many experimental results have shown that this phenomenon establishes a discontinuity on the temperature between two dissimilar materials [42]. This temperature jump characterizes the interfacial resistance to the thermal flow and is usually described by means of the interfacial thermal resistance R defined by

$$R = \lim_{\substack{\delta \to 0 \\ k_2 \to 0}} \frac{\delta}{k_2}, \tag{3.39}$$

where $\delta \equiv \sqrt{a_2^2 - a_1^2} = \sqrt{b_2^2 - b_1^2}$ (see the caption of Fig. 3.9). Note that (3.39) differs slightly from the usual definition of R, where the parameter δ is the constant

thickness of the coating layer [8]. In the present case, even though the modeling of the particles as confocal spheroids (see Fig. 3.9b) has allowed us to determine the temperature profiles and the effective thermal conductivity of the composites analytically, the thickness of the coating layer is not constant. Therefore despite (3.51) provides a convenient form of introducing the interfacial thermal resistance, it introduces a small variation in R due to the generic geometry of the particles we chose in this study. Equation (3.51) combines the geometry and the thermal conductivity of the coating layer in just one parameter, which takes into account the interfacial mismatch between the phonons of the matrix and metallic particles. Under these conditions, the coating layer disappears, the inner and outer spheroids have the same geometry, and therefore they have the same geometrical factors ($L_{ii}^{(1)} = L_{ii}^{(2)} \equiv L_{ii}$), the phases of the composite shown in Fig. 3.9a, b decrease to only two constituents, and (3.33c) reduces to

$$k_{ii} = \frac{k_1}{1 + Rk_1L_{ii}(2/a_1 + 1/b_1)}, \tag{3.40}$$

which, in absence of the interfacial thermal resistance, is equal to k_1. The combination of (3.33b) and (3.40) yields

$$\beta_{ii} = \frac{(1 - a_k\gamma L_{ii})k_1 - k_3}{[1 + a_k\gamma(1 - L_{ii})]k_1 + (1 - L_{ii})k_3}, \tag{3.41}$$

where $\gamma = 2/a_1 + 1/b_1$ and $a_K = Rk_3$ is the so-called Kapitza radius [8, 44]. This radius a_K can be interpreted as the equivalent thickness of a layer of the matrix around the spheroidal particles, with a thermal resistance $R = a_K/k_3$. It is important to note that in this limit and in absence of the effect of the electron–phonon coupling ($\chi = 1$) (3.38a) and (3.38b) reduce to the results derived by Nan et al. [8].

To have further insights on the predictions of (3.38a), (3.38b), (3.40) and (3.41), we analyze the following four limiting cases of potential interest:

3.3.1.1 Spherical Particles: $a_1 = b_1$

In this case, $L_{11} = L_{33} = 1/3$, and both (3.38a) and (3.38b) become independent of the direction parameter γ and reduce to

$$\frac{K_{11}^*}{k_3} = \frac{K_{22}^*}{k_3} = \frac{k_1(1 + 2r) + 2k_3 + 2[k_1(1 - r) - k_3]f}{k_1(1 + 2r) + 2k_3 - [k_1(1 - r) - k_3]f}, \tag{3.42}$$

where $k_1 = (k_e + k_p)/\chi$ and $r = a_K/a_1$. In absence of the coupling factor ($\chi = 1$), (3.54) reduces to the result derived by Hasselman and Johnson [5] and Nan et al. [8].

3.3.1.2 Aligned Cylindrical Particles: $a_1 \ll b_1$

For large cylinders aligned parallel to the z axis ($\theta = 0$), $L_{11} = 1/2$, $L_{33} = 0$ and (3.38a) and (3.38b) take the form

$$\frac{K_{11}^*}{k_3} = \frac{K_{22}^*}{k_3} = \frac{k_1(1+r) + k_3 + [k_s(1-r) - k_3]f}{k_1(1+r) + k_3 - [k_s(1-r) - k_3]f}, \tag{3.43a}$$

$$K_{33}^* = k_3(1-f) + k_1 f, \tag{3.43b}$$

In the absence of the coupling factor ($\chi = 1$), (3.43a) reduces to the results presented by Hasselman and Johnson [5] and Nan et al. [8], and (3.43b) is just the simple mixture rule for inclusion arranged in series, as shown by Torquato [2].

Note that a common feature of the effective thermal conductivities of composites reinforced with spheres and cylinders ((3.42) and (3.43a)) is that they both reduce the thermal conductivity of the matrix, independently of the volume fraction of the particles, for a critical radius $a_1 = a_c$ defined by $k_1/k_3 = 1/(1-r)|_{a_1=a_c}$. This relation implies

$$r_c \equiv \frac{a_K}{a_c} = 1 - \chi_c \frac{k_3}{k_s}, \tag{3.44}$$

where $k_s = k_e + k_p$ and χ_c is defined in (3.33f) for $a_1 = a_c$. In terms of the critical ratio r_c, both (3.42) and (3.43a) can be rewritten in the following compact form

$$\frac{K^*}{k_3} = \frac{1 + \sigma\lambda f}{1 - \lambda f}, \tag{3.45}$$

where $\sigma = 1$ and 2, for cylinders and spheres, respectively; and

$$\lambda = \frac{(1-r)\chi_c - (1-r_c)\chi}{(1+\sigma r)\chi_c + \sigma(1-r_c)\chi}, \tag{3.46}$$

Equations (3.44)–(3.46) express that the thermal conductivity of composites reinforced with spheres or cylinders, is totally ruled by the relative radius of these particles with respect to their critical radius a_c, the Kapitza radius a_K and the coupling length d, involved in the parameters χ and χ_c. This shows explicitly that the behavior of K^* is determined by the size scale of the particles. Note that in absence of the interfacial thermal resistance ($r = r_c = 0$), (3.46) reduces to $\lambda = (\chi_c - \chi)/(\chi_c + \sigma\chi)$, which; in contrast to the models developed under the Fourier law approach [1, 2, 4, 5, 12], still depends on the particle size. This reaffirms that not only the interfacial thermal resistance but also the coupling term has an important effect on the thermal conductivity of composites.

The critical radius a_c is determined by (3.44), which in general cannot be solved analytically (see (3.33f)). However if $a_c \ll d$, $\chi_c \approx 1 + k_e/k_p$ and (3.44) yields

$$r_c \equiv \frac{a_k}{a_c} = 1 - \frac{k_3}{k_s}\left(1 + \frac{k_e}{k_p}\right), \tag{3.47a}$$

which indicates that the critical radius a_c is independent of the coupling length d, and is greater than the Kapitza radius a_k ($a_c > a_k$). On the other hand, for $a_c \gg d$, $\chi_c \approx 1 + (k_e/k_p)/(a_c/d - 1)$ and (3.44) roughly reduces to

$$a_c = \frac{1}{k_s/k_3 - 1}\left(\frac{k_s}{k_3}a_K + \frac{k_e}{k_p}d\right). \tag{3.47b}$$

Equation (3.47b) shows a linear dependence of the coupling length d and suggests that a_c can be interpreted as a weighted average between the Kapitza radius a_c, and d; where the weights are determined by the ratios of thermal conductivities. In general, (3.47a) and (3.47b) establish the minimal and maximum values of the critical radius, respectively.

3.3.1.3 Aligned Flat Plates: $a_1 \gg b_1$

When the particles are laminate flat plates oriented perpendicular to the z axis ($\theta = 0$), $L_{11} = 0$, $L_{33} = 1$, and (3.38a) and (3.38b) becomes

$$K^*_{11} = k_3(1 - f) + \frac{k_s}{\chi}f, \tag{3.48a}$$

$$\frac{1}{K^*_{33}} = \frac{1 - f}{k_3} + (\chi + \rho)\frac{f}{k_s}, \tag{3.48b}$$

where $\rho = Rk_s/b_1$. Without taking into account the effect of the coupling factor ($\chi = 1$), the (3.48a) and (3.48b) are identical to the results derived by Torquato [2] and Nan et al. [8].

It is important to note that even though the coupling factor G could be different for spherical, cylindrical and flat plates particles, the obtained results remains valid when an average value of G is used, for each case; as explained in the text underneath (3.15b).

3.3.1.4 Randomly Oriented Spheroidal Particles

This case can be modeled by averaging the direction parameter γ over all possible orientations of the spheroidal particles ($0 \leq \theta \leq \pi/2$). The calculation of this average is straightforward and is found to be $< \gamma > = 1/3$. After inserting this value into (3.38a) and (3.38b), both equations reduces to

$$\frac{K^*}{k_3} = \frac{3 + [2\beta_{11}(1 - L_{11}) + \beta_{33}(1 - L_{33})]f}{3 - [2\beta_{11}L_{11} + \beta_{33}L_{33}]f}, \tag{3.49}$$

which is the generalization of the Maxwell result [3], for isotropic composites with spheroidal particles. Given that the leading coefficients of the volume fraction f (the quantities in square brackets) in the numerator and denominator of (3.49) are different, the concept of critical radius as was defined by spherical and cylindrical particles, cannot be applied to the case of general spheroidal particles.

3.3.2 Numerical Results and Discussions

First of all, we would like to note the validity of our model. Given that the microscopic electron–phonon interactions requires a space to take place, in general, the TTM is suitable to study the heat conduction in materials with a physical size greater than the mean free path (MFP) of the energy carriers ($2a_1$, $2b_1 >$ MFP). This constraint was the assumption made by Qiu and Tien [31] to derived this model from the Boltzmann transport equation, by evaluating its scattering term using quantum mechanical and statistical considerations. It was found that the coupling length d for a wide variety of metals (as the copper, silver, gold and others) is of the order of hundreds of nanometers (10^{-7} m) [28, 31], and the mean free path of the energy carriers is of the order of nanometers (10^{-9} m) [18] at room temperature. Usually the phonon mean free path, in the order of a few nanometers to tens of nanometer, [45–47] is much longer than the electron mean free path, which could pose constraints on the validity of the model. However, by taking into account the interfacial phonon thermal resistance, the TTM could be extended into a validity regime for spheroidal particles with sizes as small as 5×10^{-9} m [48, 49]. We thus can conclude that the model could be useful for studying the impact of electron–phonon coupling effect on the thermal conductivity of metal-nonmetal materials with a thickness as small as a few nanometers.

The results presented in Sect. 3.3.1 indicate that the major differences of thermal conductivity of metal-nonmetal composites with previously published results is given by the parameter χ, which introduces the effects of the electron–phonon coupling through: (1) the ratio between one semi-axis (size) of the spheroids and their associate coupling length, and (2) the ratio between the electron and phonon thermal conductivities (see (3.33f)). For the limiting case where the particles are nonmetallic, $k_e/k_p << 1$ or $d \to \infty$ ($G \to 0$), χ reduces to unity ($\chi = 1$), which is its value used under the Fourier approach, and (3.42)–(3.49) reduce to the results obtained by Nan et al. [8]. However, when the particles are metallic ($\chi > 1$), (3.42)–(3.49) exhibit remarkable differences with those results.

Figure 3.11 shows the coupling term χ as a function of the relative size of the particles. Note that the effects of the coupling factor G can only be neglected ($\chi \to 1$) if the dimensions of the spheroidal particles are much larger than the

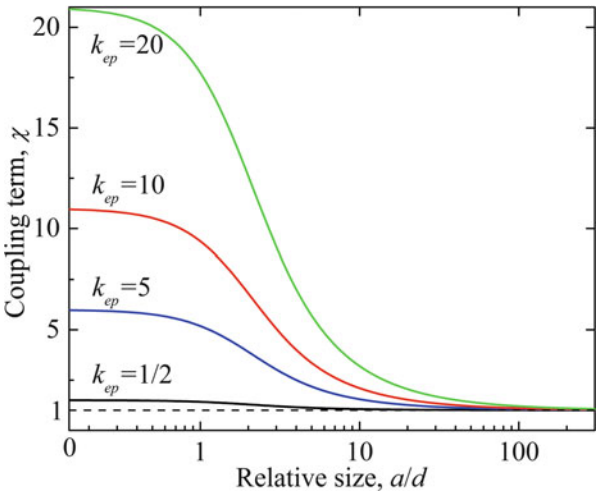

Fig. 3.11 The normalized coupling term χ as a function of the relative size of the spheroidal particles, for different $k_{ep} = k_e/k_p$ values. $a = a_{1\ \text{for}}$ prolate spheroids, and $a = b_1$ for oblate spheroids

coupling length ($a \gg d$). However, as size of these particles becomes of the same order or smaller than the coupling length ($a \leq d$), the coupling term increases and tends to the limit of $\chi \to 1 + k_e/k_p$, when $a \ll d$. This indicates that the effects of χ should be considered, especially when the electron thermal conductivity is much greater than the phonon thermal conductivity ($k_e >> k_p$), as is the case of metallic particles. Taking into account that for most metals the coupling length is of the order of hundreds of nanometers ($d \sim 10^{-7}$ m) [28, 31], Fig. 3.11 shows that the Fourier law-based models fail when one is dealing with composites with metallic nanoparticles. Another important parameter that determines the effective thermal conductivity of composites involving spherical and cylindrical particles is given by the critical radius a_c, defined in (3.44). Figure 3.12 shows that a_c increases with the Kapitza radius and decreases when the ratio k_s/k_3 of thermal conductivities increases. a_c reaches its minimal value $a_{c,\min} = a_K$ when $k_s/k_3 \to \infty$. This behavior of a_c with a_k indicates that the composites thermal conductivity decreases as a_c increases.

Figure 3.13 shows the influence of the relative particle size with respect to the coupling length on the effective thermal conductivity as a function of the volume fraction of spherical particles. Even though the derived formulas are likely not valid for high volume fractions ($f \to 1$), the lines for the entire range of values of the volume fraction has been plotted simply for completeness. Note that the thermal conductivity of the composite increases when the normalized radius a/d of the spheres increases, such that for $a/d \to \infty$, the thermal conductivity reaches its maximum values, which is predicted by the Fourier law (see Fig. 3.11). As the normalized radius is scaled down, the thermal conductivity of the composite decreases, and it reaches its minimal value for $a/d = 0$. The change of the composite thermal conductivity due to the relative size of the spheres with respect to the coupling length is bounded by $K^*|_{a/d=0} \leq K^* \leq K^*|_{a/d=\infty}$, for any value of the volume fraction. These bounds are determined by the two asymptotic values of

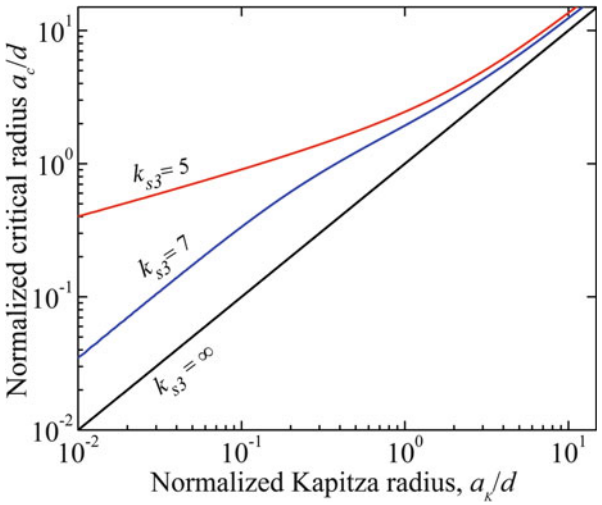

Fig. 3.12 Normalized critical radius a_c/d, as a function of the normalized Kapitza radius a_k/d and the ratio $k_{s3} = k_s/k_3$. Calculations were performed for $k_e/k_p = 4$

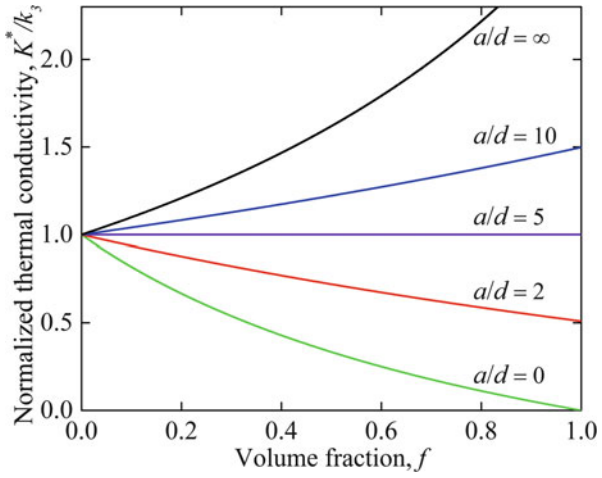

Fig. 3.13 Normalized thermal conductivity of composites with spherical particles as a function of their volume fraction, for different values of the normalized radius a/d. Calculations were performed using $a_c = 5d$, $a_k = 2d$ and $k_e = 3k_p$

the coupling term $\chi = 1,\ 1 + k_e/k_p$. Note that $K^* > k_3$ for $a > a_c$, $K^* < k_3$ when $a < a_c$, and $K^* = k_3$ at $a = a_c$, for any volume fraction. These features of the effective thermal conductivity are true for any value of the critical and Kapitza radii (see Fig. 3.14a), and they are not only valid for the case of spheres but also for cylinders, as can be shown from (3.45) and (3.46). This indicates that to increase the thermal conductivity of the matrix, the thermal and geometrical properties have to be selected such that, the radius of the particles is larger than their critical radius.

The normalized thermal conductivity of composites with spherical particles as a function of their normalized radius and Kapitza radius is shown in Fig. 3.14a, b, respectively; by comparing the predictions of the proposed approach in presence (solid lines) and absence (dashed lines) of the electron–phonon coupling

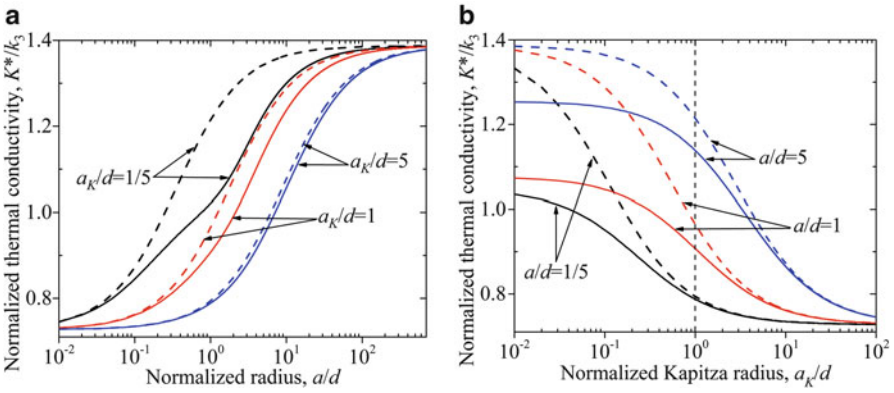

Fig. 3.14 Normalized thermal conductivity of composites as a function of (**a**) the normalized radius of the spherical particles, and (**b**) the normalized Kapitza radius, for different values of the Kapitza and particle radius, respectively. The *continuous* and *dashed lines* correspond to the predictions of the proposed model in presence and absence of the electron–phonon coupling, respectively. Calculations were performed for $k_s = 5k_3$, $k_e = 3k_p$ and $f = 20$ %

factor G ($d = \sqrt{k_a/G}$). Figure 3.14a shows that the thermal conductivity of composites is strongly determined by the size of the particles and the Kapitza radius with respect to the coupling length. For a particle radius of the order of the coupling length ($a \sim d$), the effects of G show up remarkably when the Kapitza radius is comparable or smaller than the coupling length ($a_K \leq d$). On the other hand, according to Fig. 3.14a, b, for a fixed Kapitza radius $a_K > d$, those effects become remarkable for a particle radius inside the interval $d \leq a \leq 10d$, and they reduce for other particles sizes. Based on these remarks, it is clear that the contribution of the coupling factor, for particles sizes within this interval ($d \leq a \leq 10d$), is not only present for a small Kapitza radius ($a_K \leq d$) but also for large values ($a_K > d$). Taking into account that the typical values of the coupling length and Kapitza radius are $d \sim a_K \sim 10^{-7}$ m for metal-dielectric interfaces; this indicates that the effect of the electron–phonon coupling on the thermal conductivity of composites could be observed for the case of micro-sized metallic particles, and possibly be overshadowed by the interfacial thermal resistance for nanoparticles.

Figure 3.15a–c show the effective thermal conductivity as a function of the volume fraction of the particles. The comparison of the effective thermal conductivity k of a composite, predicted by the current approach, the models by Nan et al. [8] and by Duan and Karihaloo [12] is shown in Fig. 3.15a, for two relative values of the coupling length d with respect to the radius a of the spherical particles. For a fixed particle radius, k increases when the coupling length decreases, such that for $d \ll a$, it approaches to the predictions of the Nan et al. and Duan and Karihaloo models. Figure 3.15b, c show that the change of the composites thermal conductivity with the volume fraction of randomly oriented oblate (pancake-shaped) or prolate (cigar-shaped) spheroids, respectively. Note that, as in the case of spherical

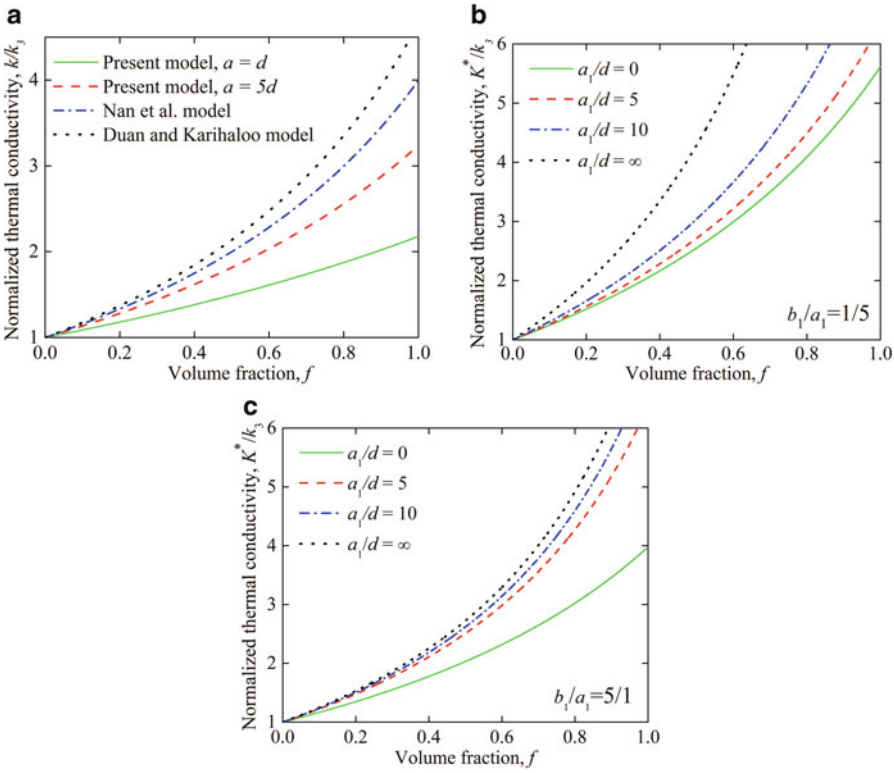

Fig. 3.15 Normalized thermal conductivity of composites as a function of the volume fraction of (**a**) spherical particles, and (**b**) and (**c**) ellipsoidal particles with aspect ratios of $b_1/a_1 = 1/5$, and $b_1/a_1 = 5/1$, respectively. Calculations were performed using $k_s = 25k_3$, $k_e = 3k_p$ and $a = 5a_K$

particles (Fig. 3.13), the effective thermal conductivity is still bounded by its lower values at $a_1/d = 0$, and higher values at $a_1/d = \infty$. This means that the effective thermal conductivity increases when the electron–phonon coupling factor G increases ($d \to 0$). The corresponding bounds associated with the oblate spheroids are higher than those of the prolate spheroids for any volume fraction. This points out that the composites with randomly oriented oblate spheroids have higher thermal conductivities than those with prolate spheroids.

The effect of the normalized thermal resistance $\rho = Rk_s/b_1$, on K^*/k_3 for oblate ($b_1/a_1 < 1$) and prolate ($b_1/a_1 > 1$) spheroids is shown in Fig. 3.16a, b, respectively. Note that when the interfacial thermal resistance is large enough, the thermal conductivity may not only increases but also decreases with the volume fraction, no matter whether the value of b_1/a_1 is 1/5 or 5. The effective thermal conductivity is largest when the interface thermal resistance is negligible, i.e. $\rho = 0$. According to Figs. 3.15b, c, and 3.16a, b, both the coupling length and the interface thermal resistances impose bounds for the maximum and minimum values of the thermal conductivity of the composite. However, while the thermal conductivity K^* of the

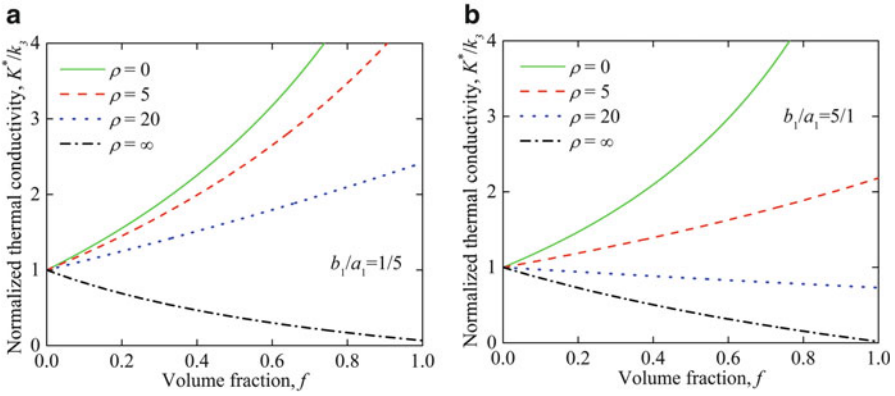

Fig. 3.16 Normalized thermal conductivity of composites as a function of volume fraction for different values of the normalized interfacial thermal resistance and aspect ratios of (**a**) $b_1/a_1 = 1/5$, and (**b**) $b_1/a_1 = 5/1$. Calculations were performed using $k_s = 25k_3$, $k_e = 3k_p$ and $a_1/d = 1/2$

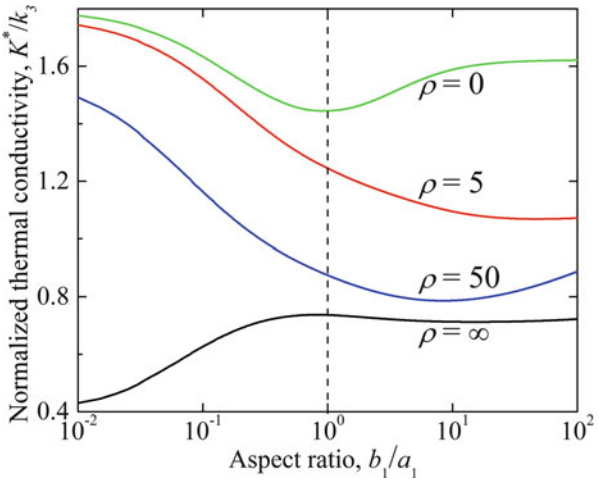

Fig. 3.17 Normalized thermal conductivity of composites as a function of the aspect ratio b_1/a_1, for different values of the normalized interfacial thermal resistance. Calculations were performed using $k_s = 25k_3$, $k_e = 3k_p$, $f = 20$ % and $a_1/d = 1/2$

composite just increases with the volume fraction, for any value of the coupling length (for $k_s > k_3$), the interfacial thermal resistance may lead to an effective thermal conductivity of the composite that is lower than the one of the matrix ($K^* < k_3$), as was reported by in the literature [8, 23, 50]. This latter feature represents a key difference between the contributions of the interfacial thermal resistance and the coupling length.

Figure 3.17 shows the thermal conductivity of composites as a function of the aspect ratio b_1/a_1 of randomly oriented spheroidal particles and the normalized interfacial thermal resistance ρ. When $\rho = 0$, the thermal conductivity of composites with oblate spheroids is larger than the one with prolate spheroids. The thermal conductivity reaches its minimum value when the particles are spherical ($b_1/a_1 = 1$).

This suggests that the thermal conductivity can be maximized if laminate flat plates are used instead of cylinders or spheres. On the other hand, in presence of the interface thermal resistance ($\rho > 0$) and for a wide range of its values, the effective thermal conductivity increases when the aspect radio b_1/a_1 decreases. However, this trend may be inverted when the interfacial thermal resistance is large enough. K^*/k_3 can be significantly modified by the shape and relative size of the particles with respect to the coupling length, and the Kapitza radius, as shown in Fig. 3.16a, b.

3.4 Composites with High Concentration of Particles

The discussions of Sects. 3.2 and 3.3 are applicable only when the interactions among the particles can be neglected. In such dilute limit, the heat flux lines generated by one particle are not distorted by the presence of the neighboring particles when the distance between neighboring particles is much larger than their size. However, for higher particle concentrations, the distance between neighboring particles can be of the order of the particle size or smaller and the interaction among particles have to be considered, which results in distortion in heat flux that is different from the prediction of the single particle assumption.

One of the first tries to address the problem of the non-dilute concentration of particles was reported by Nielsen [51], who proposed an empirical model for the thermal conductivity of composites based on the analogy between the elastic and thermal properties, which is claimed to be valid for volume fractions of particles up to their maximum packing fraction. One of the key features of this model is the introduction of the maximum volumetric packing fraction of particles, whose effects on the thermal conductivity of the composites increases with the volume fraction of the particles [51–53]. Even though the predictions of this model are in good agreement with a wide variety of experimental data involving composites with spherical and cylindrical particles [51, 52], its semi-empirical nature does make it difficult to explain how the model takes into account the particle interactions, which are strongly present at high particle concentrations. On the other hand, by using the differential effective medium theory proposed by Bruggeman [54], Norris et al. [55], Every et al. [56], and more recently Ordonez-Miranda et al. [57, 58] have reported different models that can potentially be used for the prediction of thermal conductivity in composites with high volume fractions of particles. These Bruggeman theory-based models explain clearly how the composite can be built up by means of a process of incremental homogenization, provided that the matrix remains as a continuous medium and the particles are disconnected. These models agree reasonably well with the experimental data for thermal conductivity of various composites [55–58] and porous media [59], even when the particles are non-uniform as long as the particles do not form large clusters [2, 58]. However, the Bruggeman-based models do not involve the maximum packing fraction of the particles, which plays an increasingly important role on the thermal conductivity of composites with high volume fractions of particles [51, 52]. Despite the limitations of these two approaches,

Nielsen [51] and Bruggeman-based models [55–57], represent the major efforts to describe the thermal conductivity of composites with high concentrations of particles. Thus, a more general approach that takes into account the particle interactions and the maximum packing fraction of the particles is highly desirable.

3.4.1 A Crowding Factor Model

To extend the applicability of the model developed in Sects. 3.2 and 3.3 to higher concentrations, we have recently used the concept of crowding factor to take into the particle interactions [60]. The concept of crowding factor has been introduced in economy as a population density to explain the flow of capital in open and closed economies [61]. In this area of research, the crowding factor determines how different economical agents such as the government and private entities crowd each other with similar solutions to a particular financial problem. Furthermore, the crowding factor is also involved in crowding theory of viscosity of a concentrated suspension of spherical particles [62, 63]. To take into account the particles interactions, in this theory the crowding factor γ is defined as the effective volume fraction of the suspended particles, such that spheres with a partial concentration f_1 crowd other spheres into the remaining free volume fraction $1 - \gamma f_1$. The analytical results of this theory and its generalization have shown good agreement with experimental and simulation data reported in the literature for both low and high concentrations of suspended spherical particles [63]. We extend the use of the crowding factor to describe the thermal conductivity of composites made up of particles with an arbitrary size, shape and orientation within the matrix. The effect of this factor is expected to be important at high particle concentrations, where the crowding among particles is strongly present.

As shown in Fig. 3.18, the composite with volume fraction f of particles can be viewed as embedding particles successively into the matrix with two volume fractions f_1 and f_2, i.e. $f = f_1 + f_2$. We can then analyze the effect of such a homogeneous addition. The addition of the first fraction f_1 of particles increases (or decreases) the thermal conductivity of the matrix by the factor $k_1/k_m = F(f_1)$, where k_1 and k_m are the thermal conductivities of the matrix in presence and absence of particle inclusions, respectively. When $f_1 \to 0$, the function F should reduce to a dilute-limit model. If the second fraction f_2 is added beyond the first fraction, the thermal conductivity will have a further increase (or decrease). This second addition of particles with respect to the first one is to homogeneously place particles with volume fraction f_2 in the available space not occupied by the particles with concentration f_1. By defining the crowding factor γ as the effective volume of particles per unit "real" volume of them, such as γV_1 is the effective volume of the particles in V_1, which is "seen" by the particles in V_2. Therefore, the second addition of f_2 fraction of particles further changes the effective thermal conductivity to $k/k_1 = F(f_{21})$, where $f_{21} = V_2/(V_T - \gamma V_1) = f_2/(1 - \gamma f_1)$ is the volume fraction of V_2 in the accessible volume $V_T - \gamma V_1$, where V_T is the total volume of the composite. The contribution of the crowding factor

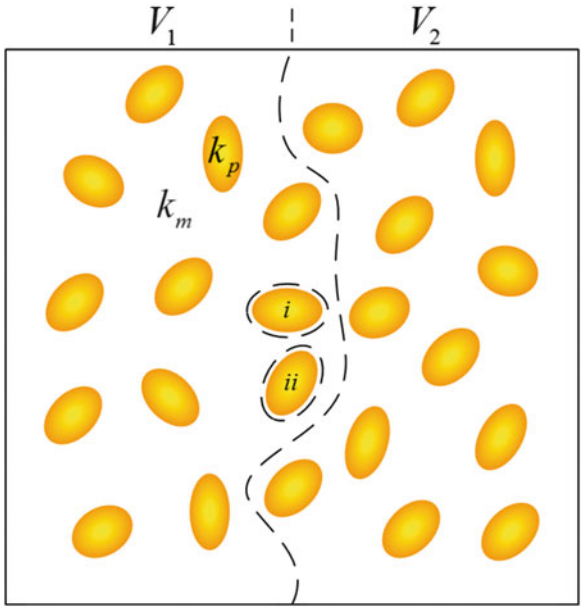

Fig. 3.18 Diagram of the composite under consideration with a total volume of particles $V_1 + V_2$

γ is particularly clear for high volume fractions of particles. For instance, given that a particle of V_2 does not fit in between particles i and ii (see Fig. 3.18), the effective volume of the particles should be slightly larger than its "real" volume. Therefore, it is expected that the parameter γ depends strongly on the geometry and maximum packing volume fraction of particles.

Taking into account that the introduction of f_2 also reduces the free volume available for f_1, the crowding factor for fractions f_1 and f_2 is mutual and therefore the effective concentration of f_1 in the composite is $f_{12} = f_1/(1 - \gamma f_2)$. To account for this mutual effect, the function $F(f_1)$ must be replaced by $F(f_{12})$. We can then determine the normalized thermal conductivity $k/k_m = (k_1/k_m)(k/k_1)$ of the composite with a total concentration $f = f_1 + f_2$ of particles by

$$F(f_1 + f_2) = F\left(\frac{f_1}{1 - \gamma f_2}\right) F\left(\frac{f_2}{1 - \gamma f_1}\right), \tag{3.50}$$

which is a functional equation for the function $F(f) = k/k_m$. Equation (3.50) establishes that this function satisfies these two conditions: $F(0) = 1$ and $F(2x) = F^2(x/(1 - \gamma x)) > 0$, which implies that $F(f)$ is always positive. The solution of (3.1) can be determined by noting that: (1) For the limiting case of $\gamma \to 0$, (3.1) reduces to Cauchy's exponential equation [64], whose solution is given by $F(x) = \exp(Cx)$, where C is an arbitrary constant. (2) Based on this asymptotic solution and on the Wentzel-Kramers-Brillouin-Jeffreys method [65], which is usually applied to solve the one-dimensional

Schrodinger equation with a position-dependent potential, the general solution of (3.1) when $\gamma \neq 0$ can be written as

$$F(f) = \exp(CfG(f)), \tag{3.51}$$

where the function $G(f)$ reduces to the unity when the parameter $\gamma = 0$. By combining (3.50) and (3.51), it is found that G satisfies a functional equation, which for $f_1 = f_2 = x$, takes the form

$$G(2x) = \frac{1}{1-\gamma x} G\left(\frac{x}{1-\gamma x}\right). \tag{3.52}$$

Since $G(f)$ should be a well-behaved function of f, we can seek a solution for (3.52) in the form of

$$G(x) = \sum_{n=0}^{\infty} A_n (\gamma x)^n, \tag{3.53}$$

where $A_0 = 1$ to guarantee that (3.51) reduces to the solution of the Cauchy's exponential function for $\gamma = 0$. Equation (3.53) represents the well-known power series method, which is usually applied to find the solution of second-order ordinary differential equations [26, 66]. After inserting (3.53) into (3.52), the following relation is found for the coefficients A_n,

$$\sum_{n=0}^{\infty} A_n (2\gamma x)^n = \sum_{n=0}^{\infty} \frac{A_n (\gamma x)^n}{(1-\gamma x)^{n+1}}. \tag{3.54}$$

By applying the binomial theorem to expand the factor $(1 - \gamma x)^{-(n+1)}$ in the power series of γx, and rearranging the resulting double series in (3.54), one finds that A_n are determined by the following recurrence relation,

$$2^n A_n = \sum_{l=0}^{n} \frac{n! A_l}{l!(n-l)!}, \qquad A_0 = 1. \tag{3.55}$$

Based on mathematical induction, it is easy to find that all the coefficients determined by (3.55) are given by $A_n = 1$. This simple result transforms the right-hand side of (3.53) into a geometric series [26], which allows writing the solution of (3.52) in the closed form $G(x) = (1 - \gamma x)^{-1}$. Thus, the general solution for the function $F(f)$ of (3.50) is given by

$$F(f) = \frac{k}{k_m} = \exp\left(\frac{Cf}{1-\gamma f}\right), \tag{3.56}$$

where C is a constant that should depend on the thermal properties and the geometry of matrix and particles. Based on (3.56), it is easy to verify that

$$F(f) = \prod_{n=1}^{N} F\left(\frac{f_n}{1-\gamma(f-f_n)}\right), \tag{3.57}$$

if the volume fraction f is divided into N small fractions, such that $f = f_1 + f_2 \ldots + f_N$. This means that the functional form of (3.56) is independent of the number of small volume fractions used to derive it.

Equation (3.56) establishes that the effect of the crowding factor γ increases with the volume fraction f of the particles, as expected. Taking into account that the heat conduction through composites depends on the thermal, geometrical and interfacial properties of their components, (3.56) indicates that the combined effect of these properties can be unified in two parameters γ and C, which are usually proportional, as shown in the next section. Furthermore, according to (3.56), a higher crowding factor is expected when the thermal conductivity of the particles is higher than that of the matrix and the interfacial thermal resistance between the matrix and particles is not so high, as shown below. This is physically reasonable, given that in this case, the particles represent favorable pathways for the heat conduction through them.

The crowding factor γ should vary with f, because the physical process of filling the matrix with particles depends on their volume fraction. We can therefore re-write the crowding factor as $\gamma(f) = \gamma_0\psi(f)$, such that $\gamma(0) = \gamma_0$ ($\psi(0) = 1$). However, the constants C and γ_0, should then be determined by comparing (3.56) with a dilute-limit model, as shown in the next sub-section, to find the final form of the effective thermal conductivity at the non-dilute limit.

3.4.2 Applications

We apply the generalized crowding factor approach, as derived above, to specific model systems where a dilute-limit model of effective thermal conductivity of composites is available. After finding constants C and γ_0 for specific models, this generalization will extend the applicability range of the existing dilute-limit model for both low and high volume fractions of particle inclusions. Two composites of potential interest are dielectric or metallic particles embedded in a dielectric matrix.

3.4.2.1 Dielectric/Dielectric Composites

Typical examples of dielectric/dielectric materials are ceramic and semiconductor particles/fillers in polymer matrix. For these composites with a low volume fraction of spherical particles (dilute limit), the experimental data on the thermal conductivity agree well with the model derived by Nan et al. [8], whose result can be written as

$$\frac{k}{k_m} = \frac{1 + 2Af}{1 - Af}, \tag{3.58}$$

where

$$A = \frac{1 - \left(k_m/k_p + a_K/a\right)}{1 + 2\left(k_m/k_p + a_K/a\right)}, \tag{3.59}$$

where $a_K = Rk_m$ is the so called the Kapitza radius [8], R is the interfacial thermal resistance between the matrix and the particles of radius a. Note that the composite thermal conductivity depends equally on the ratios k_m/k_p and a_K/a of thermal conductivities and particle size with the Kapitza radius, respectively.

By expanding (3.56), for a first-order approximation (low volume fractions of particles) and comparing the obtained result with (3.58), it is found that $C = 3A$ and $\gamma_0 = A$. Therefore the thermal conductivity of the dielectric/dielectric composites for both low and high volume fractions of particles is determined by

$$\frac{k}{k_m} = \exp\left(\frac{3Af}{1 - A\psi f}\right). \tag{3.60}$$

The function $\psi(f)$ in (3.60) should also satisfy the following limiting values: $\psi(0) = 1$ and $\psi(f_0) = f_0^{-1}$, where f_0 is the maximum packing fraction of the particles. The values of f_0 are reported in literature for different types of particles and packing [51]. For instance, for spherical particles with a random distribution, $f_0 = 63.7\%$. The first of these conditions ensures the agreement between (3.58) and (3.60), at low volume fractions ($f \ll f_0$); and the second one guarantees the maximum increase (or decrease) of the thermal conductivity of the composite is at $f = f_0$ [51, 53]. This last fact can be seen in the denominator of the exponential function in (3.60), which indicates that the maximum ($A > 0$) or minimum ($A < 0$) value of the composite thermal conductivity occurs for $\psi(f_0)f_0 = 1$. The simplest function that satisfies both conditions is given by the equation of a straight line, as follows

$$\psi = 1 + \frac{(1 - f_0)}{f_0^2} f. \tag{3.61}$$

Equation (3.61) shows that the effect of the maximum packing fraction of the particles on the thermal conductivity of the composite appears through the function ψ. Even though this function is not unique, under the current approach, it is expected that (3.61) represents a good approximation given that the crowding factor $\gamma(f) = \gamma_0\psi(f)$ depends slightly on the volume fraction f, as was shown by Lewis and Nielsen [52], to modify the Kerner equation. Note also that the first-order approximation of (3.60) resembles to the semi-empirical model of these last researchers, which

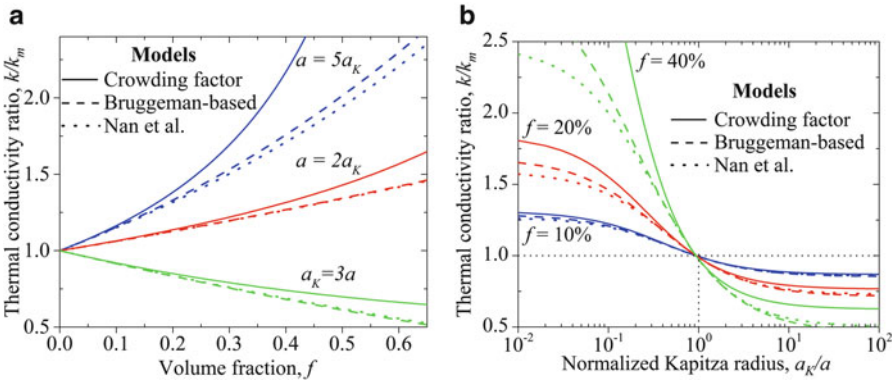

Fig. 3.19 Comparison of the predictions of the crowding factor model, a Bruggeman-based model [57] and the model by Nan et al. [8] for the thermal conductivity ratio of composites with spherical dielectric particles as a function of their (**a**) volume fraction and (**b**) normalized Kapitza radius. Calculations were performed for $k_p = 15k_m$ and $f_0 = 64$ %

indicates that the proposed approach provides a consistent extension of Nan et al. [8] and Lewis and Nielsen [52] models, who also generalize previous results.

Figure 3.19a, b shows the comparison of the predictions of the current crowding factor model, a Bruggeman-based model [57] and the model by Nan et al. [8] for the thermal conductivity of dielectric/dielectric composites with spherical particles, as a function of their volume fraction and normalized Kapitza radius, respectively.

Note that for low volume fractions of particles ($f < 15$ %), the predictions of the three models are in good agreement. For higher particles concentrations ($f > 15$ %), however, the predictions of the crowding factor model are larger than the ones of the Bruggeman-based model and the model by Nan et al., especially when the ratio a/a_K between the particle and Kapitza radii increases. This is expected for $k_p > k_m$ (in this case $k_p = 15k_m$), given that the current model takes into account the interactions among the particles through the crowding factor, which increases the overall thermal conductivity of the composite. For a particles radius of the order of or smaller than the Kapitza radius ($a/a_K = 2$, 1/3, in Fig. 3.19a), the predictions of the Bruggeman-based model and the model by Nan et al. are almost overlapped, due to the strong effect of the interfacial thermal resistance. Both the Bruggeman-based model and the crowding factor model take into account the particle interactions. However, both Fig. 3.19a, b show that predictions of the crowding factor model are larger than the ones of the Bruggeman-based model, which suggests that the crowding factor model considers a stronger contribution of the particles interactions than that of the Bruggeman-based model.

For $a_K/a < 1 - k_m/k_p$ ($a_K/a > 1 - k_m/k_p$), Fig. 3.9b shows that the composite thermal conductivity predicted by the three models increases (decreases) when the volume fraction of the particles increases, as reported in the literature [7, 40]. On the other hand, the composite thermal conductivity becomes

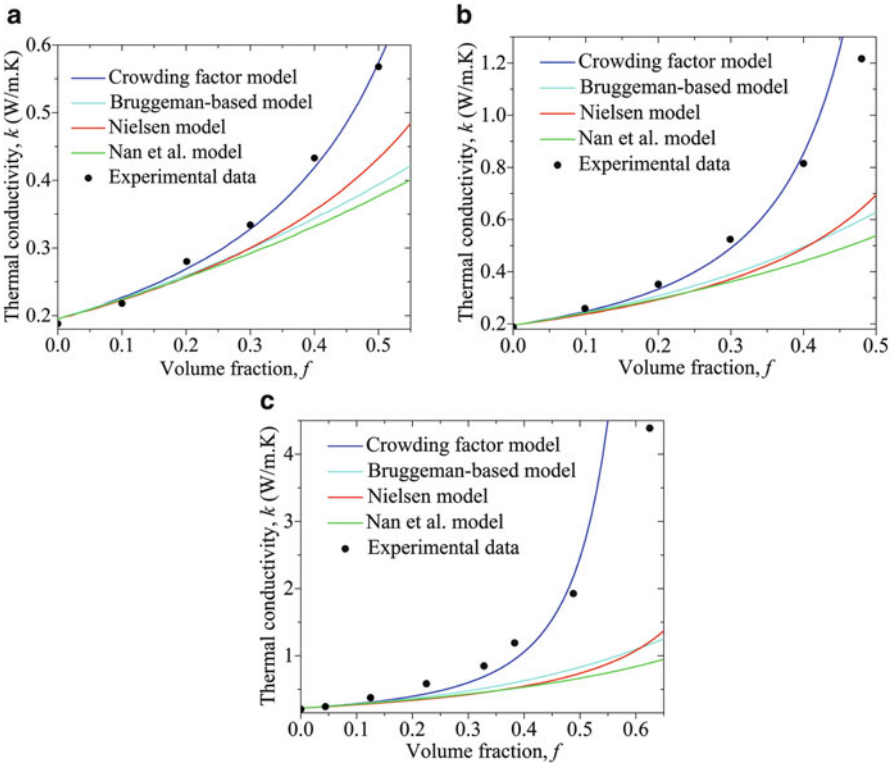

Fig. 3.20 Comparison of the theoretical curves and experimental data [67, 68] for the thermal conductivity of (**a**) silica/epoxy, (**b**) alumina/epoxy and (**c**) aluminum nitride/polyimide composites, as a function of the volume fraction of the spherical particles

independent of f and equals to the matrix thermal conductivity, for $a_K/a = 1 - k_m/k_p (=1 - 1/15$, in Fig. 3.19b).

Figure 3.20a–c shows the experimental data reported for the thermal conductivity of silica/epoxy [67], alumina/epoxy [67], and aluminum nitrate/polyimide [68] composites as a function of the volume fraction f f, in comparison with the theoretical predictions of the crowding factor model in (3.60), the Bruggeman-based model [57], the models by Nielsen [51] and Nan et al. [8]. The required physical properties at room temperature of each phase used for the calculations are given in Table 3.2. The radius of the spherical particles reported here stands for the average value.

Based on Fig. 3.20a–c, it is clear that the predictions of the three models reported in the literature remarkably underestimate the composite thermal conductivity, while the crowding factor model shows much better agreement with the experimental data. We also note that better agreements are found in Fig. 3.20a and that in Fig. 3.20c, especially for the experimental point of highest volume fraction. We can attribute the discrepancy to the fact that the aluminum nitrate particles were not

Table 3.2 Material properties used in the calculations [50, 67, 68]

Properties	k_p (W/mK)	k_m (W/mK)	a (μm)	a_K (μm)
Silica/Epoxy	1.5	0.195	13.5	1.89
Alumina/Epoxy	36	0.195	13.5	1.34
Al nitrate/Polyimide	200	0.22	2	0.146

totally spherical. The effect of particles shape becomes stronger as the volume fraction of particles increases. The good general agreement of the crowding factor model with experimental data at low as well as at high volume fractions of particles shows that this model represents a remarkable improvement with respect to the dilute-limit models, which are not able to describe the thermal conductivity of composites at high volume fractions of particles.

3.4.2.2 Metal-Nonmetal Composites

To extend the validity of the results obtained in the Sect. 3.3 to concentrations of particles up to the maximum packing fraction, we need to apply the developed crowding factor model. This can be done by equating the first-order expansion $k/k_m = 1 + Cf/(1 - \gamma_0 f)$ of the crowding factor model in (3.56) with the dilute limit model expressed in (3.38a) and (3.38b), to find the constants C and γ_0.

For the case of spherical metallic particles uniformly distributed within a dielectric matrix, this comparison applied to (3.42) and (3.56) yields $C = 3A$ and $\gamma_0 = A$, where the parameter A is determined by

$$A = \frac{1 - (\chi k_3/k_s + a_K/a)}{1 + 2(\chi k_3/k_s + a_K/a)}, \tag{3.62a}$$

$$\chi = 1 + \frac{k_e}{k_p}\frac{d}{a}\frac{i_1(a/d)}{i_1'(a/d)}, \tag{3.62b}$$

Therefore, according to (3.56), the thermal conductivity of the metallic/dielectric composite for both low and high volume fractions of particles is given by

$$\frac{k}{k_3} = \exp\left(\frac{3Af}{1 - A\psi f}\right), \tag{3.63}$$

which has the same mathematical form than (3.60), derived for dielectric/dielectric composites, but with a different parameter A.

The thermal conductivity of composites with spherical metallic particles as a function of their volume fraction and normalized radius is shown in Fig. 3.21a, b, respectively. The continuous lines correspond to the predictions of the present crowding factor model and the dashed ones to the dilute-limit result in (3.42). As expected, the predictions of the current model are larger than the ones of the

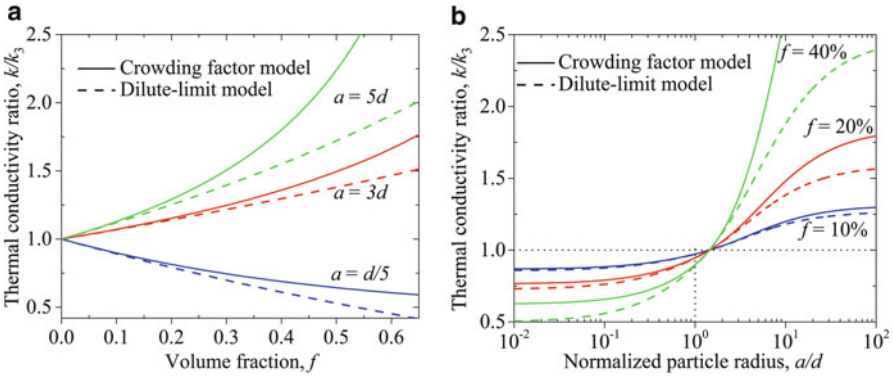

Fig. 3.21 Comparison of the predictions of the crowding factor model and the dilute-limit model for the thermal conductivity of composites with spherical metallic particles as a function of their (**a**) volume fraction and (**b**) normalized radius. Calculations were performed for $k_s = 15k_3$, $k_e = 5k_p$, $a_K = d$ and $f_0 = 64\ \%$

dilute limit model, especially when the volume fraction of the particles increases. Taking into account that the thermal conductivity of the metallic particles is usually much larger than the ones of the dielectric matrix (in this case $k_s = 15k_3$), this increase over the predictions of the dilute limit approach is due to the particle interactions, whose contribution is considered in (3.63). According to both Fig. 3.21a, b, the dilute and non-dilute approaches predict that the composites thermal conductivity increases with the particles volume fractions and size, when $a/d > (1 - \chi k_3/k_p)^{-1} a_K/d (\approx 1.5$, in this case) (see (3.62a) and (3.63)). On the other hand, for $a/d < (1 - \chi k_3/k_p)^{-1} a_K/d$, the composites thermal conductivity decreases when the particles radius decreases and/or the particles volume fraction increases.

3.5 Conclusions

The thermal conductivity of composites made up of metallic and non-metallic micro/nanoparticles embedded in a solid non-metallic matrix has been modeled and analyzed at both the dilute and non-dilute concentrations of particles. Taking into account the strong scattering of the energy carriers with the surface of the embedded nanoparticles, the thermal conductivity of nanocomposites has been determined in the dilute limit, by modifying both the thermal conductivity of the matrix and particles, accordingly. It has found that the particle shape and size dependence of the composite thermal conductivity shows up through the collision cross-section per unit volume of the particles and the mean distance that the energy carriers travel inside the particles.

The effect of the electron–phonon interactions within metallic particles shows up through the reduction of the thermal conductivity of these particles with respect to its

values obtained under the Fourier law approach. The thermal conductivity of composites with metallic particles depend strongly on (1) the relative size of the particles with respect to the intrinsic coupling length, and (2) the ratio between the electron and phonon thermal conductivities. The obtained results have shown that the particle size dependence of the composite thermal conductivity appears not only through the interfacial thermal resistance but also by means of the electron–phonon coupling.

The applicability of the proposed approach for the dilute limit has been further extended to describe the thermal conductivity of composites with particle concentrations up to the maximum packing fraction of the particles. This has been achieved by considering the particle interactions by means of the crowding factor, which is determined by the effective volume of particles. The comparison of the predictions of the crowding factor model with other non-dilute models reported in the literature has shown that this model not only generalize those models but also capture accurately the effect of the particle interactions. The predictions of the two analytical approaches proposed to describe the particle size and particle interaction effects are in good agreement with experimental and numerical data reported in the literature.

Acknowledgements We acknowledge the financial support for studying thermal and thermoelectric transport in nanostructured materials by AFOSR Thermal Science Program (Grant No. FA9550-11-1-0109), AFOSR STTR programs (PI: Dr. Sayan Naha) and DARPA ACM Program (PI: Dr. Jeff Sharp).

References

1. Milton, G.W.: The Theory of Composites. Cambridge University Press, Cambridge, NY (2002)
2. Torquato, S.: Random Heterogeneous Materials. Springer, New York (2001)
3. Maxwell, J.C.: Electricity and Magnetism. Clarendon, Oxford (1873)
4. Benveniste, Y.: Effective thermal-conductivity of composites with a thermal contact resistance between the constituents—nondilute case. J. Appl. Phys. **61**, 2840–2843 (1987)
5. Hasselman, D.P.H., Johnson, L.F.: Effective thermal-conductivity of composites with interfacial thermal barrier resistance. J. Compos. Mater. **21**, 508–515 (1987)
6. Nan, C.W., Jin, F.S.: Multiple-scattering approach to effective properties of piezoelectric composites. Phys. Rev. B **48**, 8578–8582 (1993)
7. Nan, C.W.: Effective-medium theory of piezoelectric composites. J. Appl. Phys. **76**, 1155–1163 (1994)
8. Nan, C.W., Birringer, R., Clarke, D.R., Gleiter, H.: Effective thermal conductivity of particulate composites with interfacial thermal resistance. J. Appl. Phys. **81**, 6692–6699 (1997)
9. Khitun, A., Balandin, A., Liu, J.L., Wang, K.L.: In-plane lattice thermal conductivity of a quantum-dot superlattice. J. Appl. Phys. **88**, 696–699 (2000)
10. Duan, H.L., Karihaloo, B.L., Wang, J., Yi, X.: Effective conductivities of heterogeneous media containing multiple inclusions with various spatial distributions. Phys. Rev. B. **73**, 174203–174215 (2006)
11. Prasher, R.: Thermal conductivity of composites of aligned nanoscale and microscale wires and pores. J. Appl. Phys. **100**, 034307–034315 (2006)
12. Duan, H.L., Karihaloo, B.L.: Effective thermal conductivities of heterogeneous media containing multiple imperfectly bonded inclusions. Phys. Rev. B. **75**, 064206–064214 (2007)

13. Minnich, A., Chen, G.: Modified effective medium formulation for the thermal conductivity of nanocomposites. Appl. Phys. Lett. **91**, 073105–073107 (2007)
14. Tian, W.X., Yang, R.G.: Thermal conductivity modeling of compacted nanowire composites. J. Appl. Phys. **101**, 054320–054324 (2007)
15. Jeng, M.S., Yang, R.G., Song, D., Chen, G.: Modeling the thermal conductivity and phonon transport in nanoparticle composites using Monte Carlo simulation. J. Heat Trans. Trans. ASME **130**, 042410–042420 (2008)
16. Yang, R.G., Chen, G.: Thermal conductivity modeling of periodic two-dimensional nanocomposites. Physical. Rev. B **69**, 10 (2004)
17. Chen, G.: Thermal conductivity and ballistic-phonon transport in the cross-plane direction of superlattices. Physical. Rev. B **57**, 14958–14973 (1998)
18. Kittel, C.: Introduction to Solid State Physics, 8th edn. Wiley, Hoboken, NJ (2005)
19. Tian, W.X., Yang, R.G.: Phonon transport and thermal conductivity percolation in random nanoparticle composites. Comput. Model. Eng. Sci. **24**, 123–141 (2008)
20. Tian, W.X., Yang, R.G.: Effect of interface scattering on phonon thermal conductivity percolation in random nanowire composites. Appl. Phys. Lett. **90**, 263105–263108 (2007)
21. Yang, R.G., Chen, G., Dresselhaus, S.M.: Thermal conductivity of simple and tubular nanowire composites in the longitudinal direction. Phys. Rev. B **72**, 125418–125424 (2005)
22. Prasher, R.: Thermal boundary resistance of nanocomposites. Int. J. Heat Mass. Tran. **48**, 4942–4952 (2005)
23. Ordonez-Miranda, J., Yang, R.G., Alvarado-Gil, J.J.: On the thermal conductivity of particulate nanocomposites. Appl. Phys. Lett. **98**, 233111–233113 (2011)
24. Chen, G.: Nanoscale Energy Transport and Conversion: A Parallel Treatment of Electrons, Molecules, Phonons, and Photons. Oxford University Press, Oxford. New York (2005)
25. Flammer, C.: Spheroidal Wave Functions. Dover Publications, Mineola, N.Y. (2005)
26. Arfken, G.B., Weber, H.J.: Mathematical Methods for Physicists, 6th edn. Elsevier, Boston (2005)
27. Balandin, A.A.: Thermal properties of graphene and nanostructured carbon materials. Nat. Mater. **10**, 569–581 (2011)
28. Majumdar, A., Reddy, P.: Role of electron-phonon coupling in thermal conductance of metal-nonmetal interfaces. Appl. Phys. Lett. **84**, 4768–4770 (2004)
29. Kaganov, M.I., Lifshitz, I.M., Tanatarov, M.V.: Relaxation between electrons and crystalline lattices. Sov. Phys. JETP **4**, 173–178 (1957)
30. Anisimov, S.I., Kapeliovich, B.L., Perelman, T.L.: Electron emission from metals surfaces exposed to ultra-short laser pulses. Sov. Phys. JETP **39**, 375–377 (1974)
31. Qiu, T.Q., Tien, C.L.: Heat-transfer mechanisms during short-pulse laser-heating of metals. J. Heat Tran. Trans. ASME **115**, 835–841 (1993)
32. Lin, Z., Zhigilei, L.V., Celli, V.: Electron-phonon coupling and electron heat capacity of metals under conditions of strong electron-phonon nonequilibrium. Phys. Rev. B **77**, 075133–075149 (2008)
33. Luh, D.A., Miller, T., Paggel, J.J., Chiang, T.C.: Large electron-phonon coupling at an interface. Phys. Rev. Lett. **88**, 256802–256805 (2002)
34. Melnikov, D.V., Fowler, W.B.: Electron-phonon interaction in a spherical quantum dot with finite potential barriers: The Frohlich Hamiltonian. Phys. Rev. B **64**, 245320–245328 (2001)
35. Byerly, W.E.: An Elementary Treatise on Fourier's Series and Spherical, Cylindrical, and Ellipsoidal Harmonics, with Applications to Problems in Mathematical Physics. Dover Publications, Mineola, NY (2003)
36. Hopkins, P.E., Kassebaum, J.L., Norris, P.M.: Effects of electron scattering at metal-nonmetal interfaces on electron-phonon equilibration in gold films. J. Appl. Phys. **105**, 023710–023717 (2009)
37. Mahan, G.D.: Kapitza thermal resistance between a metal and a nonmetal. Phys. Rev. B **79**, 075408–075413 (2009)

38. Sergeev, A.V.: Electronic Kapitza conductance due to inelastic electron-boundary scattering. Phys. Rev. B **58**, 10199–10202 (1998)
39. Landau, L.D., Lifshits, E.M., Pitaevskii, L.P.: Electrodynamics of Continuous Media, 2nd edn. Pergamon, Oxford, New York (1984)
40. Ordonez-Miranda, J., Yang, R.G., Alvarado-Gil, J.J.: A model for the effective thermal conductivity of metal-nonmetal particulate composites. J. Appl. Phys. **111**, 044319–044330 (2012)
41. Goldstein, H., Poole, C.P., Safko, J.L.: Classical Mechanics, 3rd edn. Addison-Wesley, San Francisco (2002)
42. Swartz, E.T., Pohl, R.O.: Thermal-resistance at interfaces. Appl. Phys. Lett. **51**, 2200–2202 (1987)
43. Swartz, E.T., Pohl, R.O.: Thermal boundary resistance. Rev. Mod. Phys. **61**, 605–668 (1989)
44. Davis, L.C., Artz, B.E.: Thermal-conductivity of metal-matrix composites. J. Appl. Phys. **77**, 4954–4960 (1995)
45. Kanskar, M., Wybourne, M.N.: Measurement of the acoustic-phonon mean free-path in a freestanding metal-film. Phys. Rev. B **50**, 168–172 (1994)
46. Stojanovic, N., Maithripala, D.H.S., Berg, J.M., Holtz, M.: Thermal conductivity in metallic nanostructures at high temperature: electrons, phonons, and the Wiedemann-Franz law. Phys. Rev. B **82**, 075418–075426 (2010)
47. Chantrenne, P., Raynaud, M., Baillis, D., Barrat, J.L.: Study of phonon heat transfer in metallic solids from molecular dynamic simulations. Microscale Thermophys. Eng. **7**, 117–136 (2003)
48. Chen, G., Zeng, T.F.: Nonequilibrium phonon and electron transport in heterostructures and superlattices. Microscale Thermophys. Eng. **5**, 71–88 (2001)
49. Zeng, T.F., Chen, G.: Phonon heat conduction in thin films: impacts of thermal boundary resistance and internal heat generation. J. Heat Tran. Trans. ASME **123**, 340–347 (2001)
50. Hasselman, D.P.H., Donaldson, K.Y., Liu, J., Gauckler, L.J., Ownby, P.D.: Thermal-conductivity of a particulate-diamond-reinforced cordierite matrix composite. J. Am. Ceram. Soc. **77**, 1757–1760 (1994)
51. Nielsen, L.E.: The thermal and electrical conductivity of two-phase systems. Ind. Eng. Chem. Fund. **13**, 17–20 (1974)
52. Lewis, T.B., Nielsen, L.E.: Dynamic mechanical properties of particulate-filled composites. J. Appl. Polym. Sci. **14**, 1449–1471 (1970)
53. Nielsen, L.E.: Generalized equation for elastic moduli of composite materials. J. Appl. Phys. **41**, 4626–4627 (1970)
54. Bruggeman, D.A.G.: Calculation of various physics constants in heterogenous substances. I. Dielectricity constants and conductivity of mixed bodies from isotropic substances. Annalen Der Physik **24**, 636–664 (1935)
55. Norris, A.N., Sheng, P., Callegari, A.J.: Effective-medium theories for two-phase dielectric media. J. Appl. Phys. **57**, 1990–1996 (1985)
56. Every, A.G., Tzou, Y., Hasselman, D.P.H., Raj, R.: The effect of particle-size on the thermal-conductivity of Zns diamond composites. Acta Metall. Mater. **40**, 123–129 (1992)
57. Ordonez-Miranda, J., Alvarado-Gil, J.J.: Thermal conductivity of nanocomposites with high volume fractions of particles. Compos. Sci. Technol. **72**, 853–857 (2012)
58. Ordonez-Miranda, J., Alvarado-Gil, J.J., Medina-Ezquivel, R.: Generalized bruggeman formula for the effective thermal conductivity of particulate composites with an interface layer. Int. J. Thermophys. **31**, 975–986 (2010)
59. Bussian, A.E.: Electrical conductance in a porous-medium. Geophysics **48**, 1258–1268 (1983)
60. Ordonez-Miranda, J., Yang, R.G., Alvarado-Gil, J.J.: A crowding factor model for the thermal conductivity of particulate composites at non-dilute limit. J. Appl. Phys. **114**, 064306–064312 (2013)
61. Chang, W.-y., Tsai, H.-f., Lai, C.-C.: Imperfect competition and crowding out. Econ. Lett. **41**, 73–79 (1993)
62. Vand, V.: Viscosity of solutions and suspensions. J. Phys. Colloid Chem. **52**, 277–299 (1948)

63. Mooney, M.: The viscosity of a concentrated suspension of spherical particles. J. Colloid Sci. **6**, 162–170 (1951)
64. Aczél, J., Dhombres, J.G.: Functional Equations in Several Variables. Cambridge University Press, Cambridge (1989)
65. Hassani, S.: Mathematical Physics: A Modern Introduction to Its Foundations. Springer, New York (1999)
66. Polyanin, A.D., Zaitsev, V.F.: Handbook of Exact Solutions for Ordinary Differential Equations, 2nd edn. Chapman & Hall, Boca Raton (2003)
67. Wong, C.P., Bollampally, R.S.: Thermal conductivity, elastic modulus, and coefficient of thermal expansion of polymer composites filled with ceramic particles for electronic packaging. J. Appl. Polym. Sci. **74**, 3396–3403 (1999)
68. Wang, J.J., Yi, X.S.: Preparation and the properties of PMR-type polyimide composites with aluminum nitride. J. Appl. Polym. Sci. **89**, 3913–3917 (2003)